73-2859

WEBER, Bruce, 1941-
THE ELASTIC SCATTERING OF Co^{60} GAMMA RADIATION FROM HEAVY NUCLEI.

The City University of New York, Ph.D., 1972
Physics, nuclear

University Microfilms, A XEROX Company, Ann Arbor, Michigan

THE ELASTIC SCATTERING OF Co^{60} GAMMA RADIATION FROM HEAVY NUCLEI

by

Bruce Weber

A dissertation submitted to the Graduate Faculty in Physics in partial fulfillment of the requirements for the degree of Doctor of Philosophy, The City University of New York.

1972

This manuscript has been read and accepted for the Graduate Faculty in Physics in satisfaction of the dissertation requirement for the degree of Doctor of Philosophy.

June 22, 1972
date

Chairman of Examining Committee

June 29, 1972
date

Executive Officer

Sol Raboy

Ferdinand J. Shore
Supervisory Committee

The City University of New York

Acknowledgements

I would like to take this opportunity to thank my advisors Dr. Alden Sayres and Dr. Carroll Trail, for it is they who are most responsible for my development as a physicist.

I would also like to thank Dr. Michael Sobel and Dr. Louis Celenza for a number of useful discussions on the theoretical aspects of my thesis.

A special thanks goes to Sol Coltun who has helped me with the design and machining of my apparatus.

I would also like to thank Lee Rothman of Columbia University for helping me with all sorts of odd jobs during the course of my experiment at Columbia University.

Lastly, I would like to thank my wife, Judy, and my mother-in-law, Evelyn Berg, for having done a yeoman job in the typing, assembly, and grammatical correcting of this thesis.

Contents

List of Tables

List of Figures

List of Graphs

Introduction

Theory

When 1 MeV electromagnetic radiation passes through matter, four separate elastic scattering processes can occur. These processes can be studied by varying the wavelength of the incident radiation, the Z of the scatterer, the angle of scatter, and by measuring the degree of polarization of the scattered radiation.

The four processes are:

Nuclear Thomson scattering

Nuclear Resonance scattering

Rayleigh scattering

Delbruck scattering.

These four elastic scattering processes are coherent, coming from the same charge distribution, and thus interference between them can alter the angular distribution of any one process. Considerable accuracy, in the determination of the various scattering amplitudes, is thus very important in order that the interference phenomena can be accounted for adequately.

Nuclear Thomson scattering is electric dipole scattering by a free charge Ze with mass Am_p, in the limit that the rest mass energy of the nucleus is large compared with the energy of the incident radiation. One could consider

this to be a special case of resonance scattering in which the resonant frequency is zero (see page19). The differential cross section for this will known process is energy independent, and proportional to Z^4.

Elastic Nuclear Resonance scattering includes two very different phenomena: (a) resonance scattering for E_γ close to some nuclear level spacing (similar to atomic resonance scattering), and (b) Giant Dipole scattering for E_γ far from resonance. By far, one means far enough so that the contribution to the scattering of the resonance closest E_γ is small compared to the sum of the contributions of all of the other resonances. Levinger[1] shows 20 eV is far enough. Moon[2] has investigated the near resonance phenomenum and shows that near resonance the cross section is of the order of 1 barn. If it should appear the resonance would be characteristic of the particular target nuclei; thus, once the target is changed to some other Z, the resonance should disappear and the cross section should become markedly smaller. For Giant Dipole scattering the incident gamma ray is absorbed by the nucleus, sharing its energy with all nucleons; the protons as a group are displaced from the neutrons as a group producing a dipole configuration. Since there are strong binding forces between nucleons, an oscillating dipole is formed. This effect is important for $E_\gamma \sim$ 10-25 MeV for heavy to medium heavy nuclei. Thus at $E_\gamma \sim$ 1 MeV, one is looking at the low energy tail of this process. The cross section is adequately accounted for and is proportional to $Z^2E_\gamma^4$ (see page 33).

Rayleigh scattering, in the long wavelength limit accounts for the blue color of the sky and also for atomic resonance scattering. For $E_\gamma > m_e c^2 > E_{ionization}$ the electrons are treated as quasi-free and either radiate elasticly or inelasticly. The inelastic scattering is more probable than the elastic processes and accounts for much of the background in this experiment. Elastic scattering can, in addition, be either coherent or incoherent. For coherence the individual electron amplitudes add and the cross section is proportional to the square of the sum of the amplitudes; for incoherence there is no phase relationship between the individual amplitudes and thus the cross section is proportional to the sum of the squares of the individual amplitudes. Coherence or incoherence depends on the dimensions of the atom in relation to the wavelength of the incident radiation and on the angle of scatter for the scattered radiation. Coherent scattering is expected for forward scattering angles. Calculations including the total coherent scattering contribution for all atomic electrons has not been made; however, calculations including the K shell electrons alone have been made and establish the amplitudes to about 80% [3, 4, 5]. The differential cross section is proportional to Z^n, where n depends on the magnitude of the momentum transfer ($1.4 < n < 2.73$ for $1.17\ \text{MeV} < E_\gamma < 1.33\ \text{MeV}$). Thus, there is an energy dependence of the cross section as is determined by n.

Delbruck scattering, a process related to pair production, is scattering of light by the static nuclear coulomb

field. This field creates a virtual electron pair which in turn absorbs the incident photon, annihilates, and (in the limit of an infinitely heavy nucleus) emits in a different direction, a photon of equal energy. At energies well above electron pair production one is observing real-pair intermediate states (states in which there is enough energy to create a pair), while for energies below $2m_ec^2$ one is observing virtual-pair intermediate states (states for which there is not enough energy to create a pair). It is these virtual states which are interesting since their proposed existence is utilized to account for the observed energy shift (vacuum polarization) of the atomic state $2^2S_{1/2}$ in hydrogen and deuterium. Thus an observation of the Delbruck effect below $2m_ec^2$ would be a second verification of these virtual-pair states. This effect has been established by various approximations yielding amplitudes valid for particular energy regions (just above and just below electron pair production energies). The differential cross section is proportional to $Z^4E_\gamma^4$ and thus large electrostatic fields (high Z) enhance this small effect.

Experiment

For energies below electron pair production, Rayleigh scattering dominates the scattering, and is adequately accounted for theoretically.

For energies above electron pair production, Rayleigh scattering decreases rapidly, while Delbruck scattering in-

creases. However, the Giant Dipole Nuclear Resonance effect, which was negligible for energies around 1 MeV, becomes significant for energies around 10 MeV. In any event, for $E_\gamma > 2m_e c^2$, the imaginary part of the Delbruck amplitude dominates over the real part, and thus one learns nothing about the virtual-pair intermediate states. It should be remarked here that theoretically, evidence for the imaginary part of the scattering amplitude can be considered as evidence for the reat part, since these amplitudes are connected by dispersion relations.

Since it was the object of this experiment to study both Rayleigh and Delbruck scattering, it was decided to investigate these processes around electron pair production energies. Ideally, this experiment should be done just below $2m_e c^2$. However, as there are no commercially available sources with suitable half lives, and energies close to, but below $2m_e c^2$, it was decided to make the investigation for Co^{60} gamma ray energies.

Appendix

Number

1 Levinger, Phys. Rev., 84, 523 (11/51)

2 Moon, Proc. Phys. Soc. (Lon.), A63, 1189 (1950)

3 Brown, Peirels, and Woodward, Proc. Roy. Soc. (Lon.), A227, 51 (1954)

4 Brenner, Brown, and Woodward, Proc. Roy. Soc. (Lon.), A227, 59 (1951)

5 Brown and Mayers, Proc. Roy. Soc. (Lon.), A242, 89 (1957)

Scattering Amplitudes and Their Relative Phases

As mentioned earlier, four separate processes contribute to the observed elastic scattering cross section. The cross section is given by: $d\sigma/d\Omega = [\,|a^{NF}|^2 + |a^{F}|^2\,]$, where NF (no flip) stands for no polarization change in the scattered wave and F (flip) stands for polarization change. These amplitudes are complex, and are functions of energy and scattering angle; ie: $a^{NF}(\nu,\theta) = a_1^{NF}(\nu,\theta) + ia_2^{NF}(\nu,\theta)$, and $a^{F}(\nu,\theta) = a_1^{F}(\nu,\theta) + ia_2^{F}(\nu,\theta)$, where the subscripts 1 and 2 stand for the real and imaginary parts respectively.

Thus, one must obtain the relative phases of all four of the processes for both the flip and no flip amplitudes. Dispersion relations are used to fix the relative phases for forward scattering with no flip, and together with the amplitude calculations, help set the phases at all other angles.

The total cross section for any system consists of an elastic part and an inelastic part. The optical theorem relates the total cross section to $a_2^{NF}(\nu,0)$. Use, then of Cauchy's theorem connects $a_1^{NF}(\nu,0)$ to $a_2^{NF}(\nu,0)$. This integral is the dispersion relation for the forward scattering amplitude. Thus, if one can somehow derive the total cross section or approximate it through physical arguements, then, in principle, $a_1^{NF}(\nu,0)$, and $a_2^{NF}(\nu,0)$ can be calculated.

Knowledge, however, of the phases of $a_1^{NF}(\nu,0)$, and

$a_2^{NF}(\nu,0)$ does not directly tell us the phases of $a_1^F(\nu,0)$, and $a_2^F(\nu,0)$. The reason for this is (as will be shown later) that, at the scattering angle of zero degrees the flip amplitudes are zero. Thus, dispersion relations are not enough to fix all the phases. We will see later that these flip and no flip amplitudes are related to states of linear polarization in the following way: $a^{NF} = (a_{\parallel} + a_{\perp})/2$, and $a^F = (a_{\parallel} - a_{\perp})/2$, where $a_{\parallel}$ is the amplitude for polarization parallel and $a_{\perp}$ is the amplitude for polarization perpendicular to the scattering plane; ie: the plane formed by $\vec{k}_I$ and $\vec{k}_S$, where the $\vec{k}$'s are the momentum vectors for the incident and scattered waves. At zero degrees $a_{\parallel}$ and $a_{\perp}$ have the same sign; thus, if the relative phases of $a_{\parallel}$ and $a_{\perp}$ are known through some calculation, comparison with the dispersion calculation can establish the sign for a^F.

In Quantum Electrodynamics, the elastic cross section is always smaller than the inelastic cross section; this is because there is only one way the elastic event can occur while there are many ways for the inelastic event. Thus, the total cross section can be approximated by the inelastic part alone. As an example, consider the scattering of light by light. Elastic scattering is much less likely to occur compared with pair production. Even in the case of the scattering of light by the nuclear coulomb field, pair production is most likely to occur $\sigma_{pp} \propto Z^2 R_o^2$ although elastic (Delbruck) scattering can also occur $\sigma_{Del} \sim (Z\alpha)^4 R_o^2$. The ratio of $\frac{\sigma_{pp}}{\sigma_{Del}}$ is smallest for heavy nuclei (large Z), and in the case of lead

is 384.

Using the above arguements, we define for the no flip amplitudes (the superscript NF will be dropped for the rest of this section).

(1) the scattering amplitude is given by: $a(\nu,\theta) = a_1(\nu,\theta) + ia_2(\nu,\theta)$, where ν is the binding energy (or resonant energy) and θ is the scattering angle.

(2) the optical theorem is given by: $a_2(\nu,0) = \frac{\nu\sigma_T}{4\pi}$ where σ_T is the total cross section for scattering.

(3) the dispersion relation from Cauchy's theorem is $a_1(\nu,0) = a_1(0,0) + \frac{\nu^2}{2\pi^2}\int_0^\infty \frac{\sigma_T(\nu')}{\nu'^2-\nu^2}d\nu'$, where $a_1(0,0)$ is the free particle amplitude.

(4) the total cross section is $\sigma_T = \sigma_{Inelastic} + \sigma_{Elastic}$

(5) for Quantum Electrodynamics $\sigma_T \simeq \sigma_{IE}$ ($\sigma_{IE} >> \sigma_E$).

Thus: $a_2(\nu,0) \simeq \frac{\nu\sigma_{IE}}{4\pi}$ and a_1 is given by: $a_1(\nu,0) = a_1(0,0) + \frac{\nu^2}{2\pi^2}\int_0^\infty \frac{\sigma_{IE}(\nu')}{\nu'^2-\nu^2}d\nu'$. The imaginary part of the forward scattering amplitude is thus related to inelastic scattering processes, while the real part is related to elastic processes.

The scattering can be broken up into two parts, scattering from the bare nucleus and from the atomic electron cloud. The total real amplitude is the sum of a_1^n and a_1^a:

$a_1(\nu,0) = a^n(\nu,0) + a^a(\nu,0)$ and $a_1(\nu,0) = a^n(\nu,0) + a^a(\nu,0)$.

$a_1^n(\nu,0) = a_1^n(0,0) + \frac{\nu^2}{2\pi^2}\int_0^\infty \frac{\left[\sigma^n_{Pair}(\nu') + \sigma^n_{Photodisintegration}(\nu')\right]}{\nu'^2-\nu^2}d\nu'$.

$a_1^n(\nu,0) = a_1^n(0,0) + \frac{\nu^2}{2\pi^2}\int_0^\infty \frac{\left[\sigma^n_{Pair}(\nu') + \sigma^n_{Photodisintegration}(\nu')\right]}{\nu'^2-\nu^2}d\nu'$. The

first term, $a_1^n(0,0)$, is for a free particle of charge Ze and mass Am_p - the well known Nuclear Thomson scattering amplitude, $-(Ze)^2/Am_pc^2$ (see page 30). The term $\frac{\nu^2}{2\pi^2}\int_0^\infty \frac{\sigma_{pair}^N}{\nu'^2-\nu^2}d\nu'$ is the Delbruck contribution. This integral has been calculated by Rohrlich and Gluckstern[3]. The integral turns out to be positive for E_γ = 1.33 MeV, thus a_{1Del}^n is 180° out of phase with a_{1Th}^n.

This last term $\frac{\nu^2}{2\pi^2}\int_0^\infty \frac{\sigma_{photodisintegration}^N}{\nu'^2-\nu^2}d\nu'$, is Giant Dipole scattering[1]. This term has been calculated by Levinger[5] for $E_\gamma << E_{PD} \gtrsim 15$ MeV. From non-relativistic electromagnetic theory, one can determine the sign of a_{1PD}^n relative to a_{1Th}^n. For the case of the scattering of light by bound charges (see page 33) excluding dissipative and radiative effects, the scattering amplitude is: $a^{NF} \sim \omega^2/(\omega_o^2 - \omega^2)$, where ω_o is the binding energy (or resonant energy) and ω is the energy of the incident radiation. For Thomson scattering $\omega_o = 0$ and thus $a^{NF} < 0$, while for $\omega << \omega_o$ (well below resonance, see page 33) $a^{NF} > 0$. Thus a_{1Th}^n and a_{1PD}^n have opposite signs.

The atomic contribution is given by[1,2]:
$a_1^a(\nu,0) = a_1^a(0,0) + \frac{\nu^2}{2\pi^2}\int_0^\infty \frac{(\sigma_{pair}^a - \sigma_{ppc} + \sigma_{pe})}{\nu'^2-\nu^2}d\nu'$. For bound electrons $a_1^a(0,0)$ is zero[2].

The integral $\frac{\nu^2}{2\pi^2}\int_0^\infty \frac{\sigma_{pair}^a}{\nu'^2-\nu^2}d\nu'$ is Delbruck scattering from the atomic electron cloud. This term is a_{1Del}^n/Z^2 (ratio of the electron charge to the nuclear charge) and will be neglected.

The next term $\frac{\nu^2}{2\pi^2}\int_0^\infty \frac{(\sigma_{pe}-\sigma_{pex})}{\nu'^2-\nu^2}d\nu'$ is the Rayleigh scattering amplitude where σ_{ppc} is the cross section for pair production

in which the final electron is captured in a bound state (K shell). Classically $a^{NF} \sim \omega^2/(\omega_o^2 - \omega^2)$ and thus for $\omega > \omega_o$ ($E_\gamma > E_{ionization}$, for this experiment $E_\gamma > 1$ MeV while $\omega_o < 1$ keV) $a < 0$. This integral was calculated by Levinger and Rustgi[4] by approximating σ_{PE} by σ_{EK}. Their results for 1 MeV gamma rays scattered by mercury (also valid for lead and tin) show that a^a_{1R} is negative, agreeing with the above classical result. Thus a^a_{1R} is out of phase with a^n_{1D}. The optical theorem, then gives us the relative signs of the imaginary amplitudes by knowing the cross section. Using this, Rohrlich and Gluckstern[3] show that the imaginary part of the Delbruck scattering amplitude is positive, while Levinger and Rustgi[4] show that the same is true for the Rayleigh amplitude.

To summarize:

(1) for no polarization change:

$a^n_{1Th} < 0$

$a^n_{1Del} > 0$ $\qquad$ $a^n_{2Del} > 0$

$a^a_{1R} < 0$ $\qquad$ $a^a_{2R} > 0$

$a^n_{1NR} > 0$

(2) for polarization change:

$a^n_{1Th} > 0$

$a^n_{1Del} > 0$ $\qquad$ $a^n_{2Del} < 0$

$a^a_{1R} > 0$ $\qquad$ $a^a_2 > 0$

$a^n_{1NR} < 0$

Calculation of the Scattering Amplitudes

Introduction

In this section the classical problem of the elastic scattering of electromagnetic radiation from (a) an unbound charge (Nuclear Thomson Scattering), and (b) a bound charge (resonance scattering) will be investigated. Next, the calculations made to establish the coherent scattering by many bound charges (Rayleigh Scattering) will be reviewed. Finally, a review of the non-linear interaction of electromagnetic radiation with the nuclear coulomb field (Delbruck Scattering) will be made.

Having established the amplitudes, each subsection will end with a calculation, summarized in a table, pertinent to the scattering of Co^{60} gamma radiation from lead, tin, and mercury.

General

In general, the incident electromagnetic radiation can have two independent polarizations (as in right and left circular polarization or linear polarization parallel and perpendicular to the scattering plane). The differential cross section (for unpolarized light) is obtained by averaging over initial polarizations, and summing over final polarizations; i.e., $d\sigma/d\Omega = |a|^2 = |a^{NF}|^2 + |a^{F}|^2$, where

a is the scattering amplitude, and a^{NF} and a^{F} are respectively the amplitudes for no polarization change (no flip), and for polarization change (flip).

Of the four coherent processes present in this experiment, the major contributors behave as electric dipole radiators (see sections on Nuclear Thomson and Rayleigh scattering). By this, it is meant that the angular distribution for the power radiated (the differential cross section) is proportional to: $1 + \cos^2\theta$. The scattered dipole field is partically linearly polarized[6]; the degree of linear polarization depending on the angle of scatter (it is well known that the blue light scattered by the atmosphere is completelylinearly polarized for 90° scattering and partially polarized for all other scattering angles). Therefore, it would be advantageous to compute the scattering amplitudes for these two components of polarization; especially if any polarization measurements are to be made. However, as it is more convenient to go from the amplitudes for right and left circular polarization to the amplitudes for linear polarization than visa versa, we will calculate the former rather than the latter. Later, it will be seen that the theoretical calculations for Delbruck scattering are for final states of linear polarization, thus conversion to states of circular polarization will be necessary in order to be consistent with other theoretical calculations.

Nuclear Thomson Scattering

The classical interaction of electromagnetic radiation with an unbound (free) particle of mass Am_p, charge Ze, radius $A^{1/3}$ fm (1 fm = 10^{-13}cm; from here on, when $A^{1/3}$ is written, the units fm are to be assumed), magnetic moment $m\mu_N$ (where μ_N is the nuclear magneton), and electric quadrupole moment Q will be discussed first.

Assuming the nucleus to be massive compared to the energy of the incident radiation, $E_\gamma << Am_pc^2$, then only oscillations with amplitude $a \sim A^{1/3}$ fm about some origin take place.

As a first approximation, all intrinsic electric and magnetic moments will be neglected. Then, later, the effects of these intrinsic moments will be included.

Classically the differential cross section for the scattering of electromagnetic radiation is given by the ratio of the power radiated per unit solid angle divided by the incident energy flux[7] : $\frac{d\sigma}{d\Omega} = \frac{|\vec{H}_S \cdot \vec{H}_S^*| R_o^2}{|\vec{H}_I \cdot \vec{H}_I^*|}$ where $\vec{H}_S$ and $\vec{H}_I$ are the scattered and incident fields and R_o is the distance to the field point. The radiation field of a charge distribution Ze contains, in general, all orders of multipole radiation. However, an expansion in R_n/λ , where R_n is the size of the radiating system and λ is the wavelength of the radiation, including first order terms yields:
$\vec{H}_S = \frac{1}{c^2 R_o}\left[\ddot{\vec{d}} \times \hat{n} + \frac{1}{c}(\dddot{\vec{D}} \times \hat{n}) + (\dddot{\vec{m}} \times \hat{n}) \times \hat{n}\right]$ where the first term is the dipole contribution, the second term is the electric

quadrupole term and the third term is the magnetic dipole contribution. If R_n/λ is small, then the expansion is valid and the second and third terms should be small compared to the first. The ratio of R_n to λ for 1 MeV gamma rays on Pb is: $R_n/\lambda \sim A^{1/3}/\lambda \sim 3(10^{-2})$. Thus, the first order terms in R_n/λ are small compared with the dipole term, but at this point will not be neglected. Higher order terms $(R_n/\lambda)^m$ $(m>1)$ are even smaller and will be neglected.

The incident radiation field is given by the following expressions:

$$\vec{E}_I = \vec{E}_o e^{-i(\vec{k}\cdot\vec{r}-wt)}$$

$$\vec{H}_I = \vec{H}_o e^{-(\vec{k}\cdot\vec{r}-wt)}$$

$$|\vec{E}_o| = |\vec{H}_o|$$

$$\hat{E}_I x \hat{H}_I = \hat{k}_I$$

While the different multipole moments are given by:

electric dipole $\quad \vec{d}=Ze\vec{r}$

electric quadrupole $\quad \vec{D}=Ze(3\vec{r}(\hat{n}\cdot\vec{r}) - \hat{n}r^2)$

$$\vec{D}=\sum_{ij} D_{ij}\hat{n}_j = \sum e(3x_i x_j - \delta_{ij}r^2)\hat{n}_j$$

magnetic dipole $\quad \vec{m}=Ze(\vec{r}x\vec{v})/2c$

The equation of motion for this system of charges is given by: $Am_p\ddot{\vec{r}} = ZeE_I + Ze(\dot{\vec{r}}x\vec{H}_I)/c + Ze\vec{\nabla}\left[\sum_{ij}(3x_i x_j - \delta_{ij}r^2)\frac{\partial E_j}{\partial x_i}\Big|_{x_i=0}\right]$ The first two terms are the forces on a charged particle Ze moving with velocity $\dot{r}$ in crossed electric and magnetic fields. The third term is present due to the fact that the electric field varies over the volume of the charge distribution so that each individual charge sees a slightly different electric field.

The first term is proportional to ZeE_o, while the second is proportional to $(\dot{r}/c)ZeE_o$; but $\dot{r}/c$ is small (since $E_\gamma/Am_pc^2 \ll 1$) and thus the second term will be neglected compared with the first.

The third term is proportional to $E_oDk/r \sim ZeE_okr$ or kr times the first term. But $r \sim A^{1/3}$ and $k \sim 1/\lambda$ thus $kr \sim A^{1/3}/\lambda$. For 1 MeV gamma radiation on a nucleus of A=200, λ =930 fm and $A^{1/3} \simeq$ 6fm; therefore, $A^{1/3}/\lambda \simeq 6(10^{-3})$. Thus the third term will also be neglected, and we are left with: $Am_p\ddot{\vec{r}} \simeq Ze\vec{E}_I$.

To calculate $d\sigma/d\Omega$, we first need $\vec{H}_S$ or equivalently $\ddot{\vec{d}}$, $\dddot{\vec{D}}/c$, and $\ddot{\vec{m}}$; i.e., $\ddot{\vec{d}} = Ze\ddot{\vec{r}}$

$$\ddddot{\vec{D}}/c = (Ze/c\ [3(\dddot{\vec{r}}(\hat{n}\cdot\vec{r}) + 3\ddot{\vec{r}}(\hat{n}\cdot\dot{\vec{r}}) + 3\dot{\vec{r}}(\hat{n}\cdot\ddot{\vec{r}}) + \vec{r}(\hat{n}\cdot\dddot{\vec{r}}) - 2\hat{n}(3\dot{r}\ddot{r} - r\dddot{r})]$$

$$\ddot{\vec{m}} = Ze(\ddot{\vec{r}}\cdot\dot{\vec{r}})/2c.$$

Using the fact that $r \sim A^{1/3}$, $\dot{r} \ll c$, $\ddot{r} \sim ZeE_o/Am_p$, and $\dddot{r} \sim c\ddot{r}/\lambda$, we have: $\ddot{d} \sim Z^2e^2E_o/Am_p$

$$\dddot{D}/c \sim (Z^2e^2E_o/Am_p)\ (A^{1/3}/\lambda + \dot{r}/c)$$

$$\ddot{m} \sim (Z^2e^2E_o/Am_p)\ (\dot{r}/c).$$

But for 1 MeV gamma radiation on nuclei of A 200

$\dddot{D}/c \sim \ddot{d}(6x10^{-3}) + 10^{-5})$ and

$\ddot{m} \sim \ddot{d}(10^{-5})$ and thus both $\dddot{D}/c$ and $\ddot{m}$ are small compared to $\ddot{d}$ and will be neglected.

We are thus left with:

$$\vec{H}_S = (\ddot{\vec{d}}x\hat{n})/c^2R_o = Z^2e^2E_o(\hat{E}_Ix\hat{n})/c^2R_oAm_p \text{ or}$$

$|\vec{H}_S| = Z^2e^2E_o(\sin\Theta)/c^2R_oAm_p$, where Θ is the angle between $\vec{E}_I$ and the direction to which the scattered radiation

is being investigated, $\hat{n}$ (see diagram below).

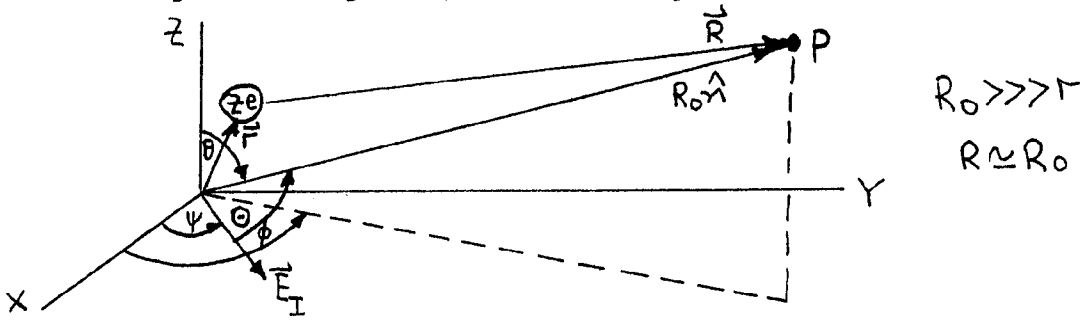

The differential cross section is thus given by:

$d\sigma/d\Omega = (Z^2e^2/Am_pc^2)^2 \sin^2\Theta$, but from the above diagram $\sin^2\Theta = 1 - (\sin^2\theta)(\cos^2(\phi - \psi))$, where ψ determines the initial polarization. For unpolarized radiation, one averages $\sin^2\Theta$ over ψ, ie:

$$(1/2\pi)\int_0^{2\pi}(\sin^2\Theta)d\psi = (1/2\pi)\int_0^{2\pi}(1 - (\sin^2\theta)(\cos^2(\phi-\psi))d\psi$$
$$= (1/2)(1 + \cos^2\theta)$$

Thus: $d\sigma/d\Omega = (Z^2e^2/Am_pc^2)^2(1/2)(1+\cos^2\theta)$. This is classical dipole (Thomson) scattering from a charge Ze and mass Am_p.

Having investigated the first approximation, the intrinsic moments will now be included. The intrinsic moments present in various isotopes of lead, tin and mercury are listed in Table 1.

Table 1

Element	m (Nuc. Magnetons)	Q (10^{-24} cm^2)	Abundance in Nature (%)
$^{65}Sn^{50}$	- .9178	-	.38
$^{67}Sn^{50}$	- .9998	-	7.6
$^{68}Sn^{50}$	-1.0460	-	8.5
$^{117}Hg^{80}$	.52	-	-
$^{119}Hg^{80}$	.504	-	16.9
$^{121}Hg^{80}$	- .599	.6	13.2
$^{125}Pb^{82}$	.5875	-	21.8

The term in $\vec{H}_S$ due to a magnetic dipole contribution is $(\ddot{\vec{m}}x\hat{n})x\hat{n}/c^2R_o$, where for an intrinsic magnetic moment $m\mu_N$, $\ddot{\vec{m}}$ is given by: $\dot{\vec{m}} = m\mu_N\alpha$, where α is the angular acceleration of the magnetic dipole vector. The angular acceleration can be defined as follows: $\vec{\Gamma} = \vec{m}x\vec{H}_I = I\vec{\alpha}$

$$|\vec{\alpha}| \simeq m\mu_N H_o/I = m\mu_N E_o/Am_p(A^{1/3})^2$$

Thus, since $\ddot{\vec{m}} = m\mu_N\alpha$, we have: $\ddot{\vec{m}} = m\mu_N(m\mu_N E_o/Am_p A^{2/3})$, where μ_N is the nuclear magneton; thus:

$|\dddot{\vec{m}}| = (Z^2e^2E_o/Am_p)(m^2h^2/4m_p^2c^2Z^2A^{2/3})$. For tin A=50, and A=115, thus $\ddot{m}_{Sn} \simeq 10^{-7}(Z^2e^2E_o/Am_p)$. This term is thus 10^{-7} times smaller than the dipole term and can be neglected.

The electric quadrupole present in $_{121}Hg^{80}$ is $.6(10^{-24})$ cm. This is now to be compared with the electric quadrupole present in the static case:

$D/e = r^2 = A^{2/3} = .24(10^{-24})$ for A=121. Thus, since the static electric quadrupole term did not contribute to H_S neither will the intrinsic quadrupole.

Classically, then, one expects elastic dipole scattering from a charge distribution Ze, with mass Am_p and that all other multipoles, whether due to an oscillating charge distribution or intrinsic moments, contribute little or nothing additional to the cross section:

$$d\sigma/d\Omega = (Z^2e^2/Am_pc^2)^2(1 + \cos^2\theta)/2.$$

This result is really the low energy limit for Compton scattering from a charge Ze with mass Am_p, and it is in this context that the particle can be considered static, and the scattering elastic. To investigate this limit, the

shift in gamma ray energy will next be calculated. The shift is given by: $\Delta E_\gamma = \Delta E_n = h\nu_o - h\nu'$

$$= h\nu_o - \frac{h\nu^o}{1 + h\nu_o(1-\cos\theta)/m_N c^2}$$

The maximum energy shift occurs for back scattering ($\theta=180°$) and thus: $\Delta E_\gamma = (2(h\nu_o)^2/m_N c^2)(1 + 2h\nu_o/m_N c^2)$. The least elastic event will occur for the lightest nuclei, which for this experiment is tin. For $E_\gamma \sim 1$ MeV one has: $\Delta E_\gamma = 20$ eV. Such a small shift in the gamma ray energy can not be detected with existing detectors. For this experiment the energy resolution of the detection system was about 3 keV, therefore a 20 eV shift was undetectable.

In addition, the Compton cross section for unpolarized light is: $d\sigma/d\Omega = (Z^2e^2/Am_pc^2)^2(\nu'/\nu_o)^2(\nu/\nu' + \nu'/\nu_o - 2\cos^2\theta)$ which reduces to the Thomson cross section calculated earlier for $\nu' = \nu$.

Having investigated just how elastic Thomson scattering is, the amplitudes corresponding to this process will next be calculated.

Earlier, it was shown that the square of the scattering amplitude is equal to the differential cross section. For Thomson scattering, the differential cross section before averaging over initial polarizations, is given by: $d\sigma/d\Omega = |a|^2 = (Z^2e^2/Am_pc^2)^2 \left|(\hat{E}_I x \hat{n}) \cdot (\hat{E}_I x \hat{n})\right|$. Thus, the scattering amplitude is given by: $a = (Z^2e^2/Am_pc^2)\left|(\hat{E}_I x \hat{n})\right|$. The vector $\hat{n}$ is a unit vector in the direction of the scattered wave, thus, $\hat{n} = \hat{k}_S$, where $\hat{k}_S = \hat{E}_S x \hat{H}_S$, and $\hat{E}_I x \hat{n} = \hat{E}_S(\hat{E}_I \cdot \hat{H}_S) - \hat{H}_S(\hat{E}_I \cdot \hat{E}_S)$.

Since all that happens in the elastic scattering process is that the momentum vector, $\vec{k}_I$, of the gamma ray is rotated through Θ degrees to $\vec{k}_S$ (with $|\vec{k}_I| = |\vec{k}_S|$), it is to be noted that $\hat{E}_I$ is perpendicular to $\hat{H}_S$ just as it is to $\hat{H}_I$. Therefore, $\hat{E}_I x \hat{n} = -\hat{H}_S(\hat{E}_I \cdot \hat{E}_S)$, and $a = -(Z^2e^2/Am_pc^2)(\hat{E}_I \cdot \hat{E}_S)$. It is appropiate to note here that if the incident and scattered polarizations are parallel (no flip) then a is negative, and if they are anti-parallel (flip) then a is positive.

Since the intention is to average over initial polarizations and sum over final polarizations, one can choose any two orthogonal polarization states to define $d\sigma/d\Omega$. Rayleigh scattering amplitudes were calculated for states of circular polarization, thus, it is convient to choose the same states for all other amplitudes.

For states of circular polarization, we have: $\hat{E}_I = (\hat{\epsilon}_1 \pm i\hat{\epsilon}_2)/\sqrt{2}$, and $\hat{E}_S = (\hat{\epsilon}'_1 \pm i\hat{\epsilon}'_2)/\sqrt{2}$, where $\hat{\epsilon}_1$ and $\hat{\epsilon}'_1$ are unit vectors perpendicular to the scattering plane, and $\hat{\epsilon}_2$ and $\hat{\epsilon}'_2$ are parallel to this plane. For no polarization flip $\hat{\epsilon}_1 \pm i\hat{\epsilon}_2$ becomes $\hat{\epsilon}'_1 \pm i\hat{\epsilon}'_2$, while for polarization flip $\hat{\epsilon}_1 \pm i\hat{\epsilon}_2$ becomes $-\hat{\epsilon}'_1 \pm i\hat{\epsilon}'_2$.

The amplitude for the scattering of unpolarized radiation is given by: $|a|^2 = |a^{NF}|^2 + |a^F|^2$, where the amplitudes a^{NF} and a^F can be written for states of circular polarization as follows:

$$a^{NF} = -(Z^2e^2/Am_pc^2)(\hat{E}_I \cdot \hat{E}_S)$$

$$= -(Z^2e^2/Am_pc^2)[(\hat{\epsilon}_1 \pm i\hat{\epsilon}_2)/\sqrt{2}] \cdot [(\hat{\epsilon}'_1 \pm i\hat{\epsilon}'_2)/\sqrt{2}]$$

$$= -(Z^2e^2/Am_pc^2)(\hat{\epsilon}_1 \cdot \hat{\epsilon}'_1 + \hat{\epsilon}_2 \cdot \hat{\epsilon}'_2)/2, \text{ and}$$

using the definitions of $\hat{\epsilon}_1$, $\hat{\epsilon}_2$, $\hat{\epsilon}'_1$, and $\hat{\epsilon}'_2$ we have:

$$a^{NF} = -(Z^2e^2/Am_pc^2)(1 + \cos\theta)/2$$

For a^F:

$$a^F = -(Z^2e^2/Am_pc^2)[(\hat{\epsilon}_1 \pm i\hat{\epsilon}_2)/\sqrt{2}]\cdot[(-\hat{\epsilon}'_1 \pm i\hat{\epsilon}'_1)/\sqrt{2}]$$

$$= -(Z^2e^2/Am_pc^2)(-\hat{\epsilon}_1\cdot\hat{\epsilon}'_1 + \hat{\epsilon}_2\cdot\hat{\epsilon}'_2)/2$$

$$= (Z^2e^2/Am_pc^2)(1 - \cos\theta)/2$$

Using these amplitudes it is straight forward to show that $d\sigma/d\Omega$ for unpolarized light results in the Thomson cross section; ie:

$$d\sigma/d\Omega = |a^{NF}|^2 + |a^F|^2$$

$$= (Z^2e^2/Am_pc^2)^2[(1+\cos\theta)^2/4 + (1-\cos\theta)^2/4]$$

$$= (Z^2e^2/Am_pc^2)^2[1 + \cos^2\theta]/2$$

Thus these amplitudes lead to the correct cross section. To summarize; the Nuclear Thomson amplitudes are given by:

$$a^{NF} = -(Z^2e^2/Am_pc^2)(1 + \cos\theta)/2$$

and

$$a^F = (Z^2e^2/Am_pc^2)(1 - \cos\theta)/2.$$

Table 2 gives the Thomson amplitudes for lead, tin, and mercury.

Table 2

Thomson Amplitudes

θ	Mercury		Lead		Tin	
	$a^{\overline{NF}}(R_o)$	$a^{F}(R_o)$	$a^{\overline{NF}}(R_o)$	$a^{F}(R_o)$	$a^{\overline{NF}}(R_o)$	$a^{F}(R_o)$
0	-.016	0	-.0162	0	-.0062	0
15	-.0157	.0003	-.016	.0003	-.006	.0001
30	-.0149	.0011	-.0151	.0011	-.0058	.0004
45	-.0136	.0023	-.0139	.0024	-.0053	.0009
60	-.012	.004	-.0122	.0041	-.0047	.0016
75	-.01	.0059	-.0102	.006	-.0039	.0023
90	-.008	.008	-.0081	.0081	-.0031	.0031
105	-.0059	.01	-.0062	.0102	-.0023	.0039
120	-.004	.012	-.0041	.0122	-.0016	.0047
135	-.0023	.0136	-.0024	.0139	-.0009	.0053
150	-.0011	.0149	-.0011	.0151	-.0004	.0058
165	-.0003	.0157	-.0003	.016	-.0001	.006
180	0	.016	0	.0162	0	.0062

(where R_o is the classical electron radius)

Nuclear Resonance Scattering

In the previous section the elastic scattering of electromagnetic radiation by an unbound charged particle was investigated. Let us now investigate the problem including binding. The force for the unbound case was shown to be $m\ddot{\vec{r}} = e\vec{E}_I$. If binding and radiative effects are now included the equation of motion becomes[8] : $m\ddot{\vec{r}} = e\vec{E}_I - k\vec{r} + \gamma\dddot{\vec{r}}$, where $k\vec{r}$ represents the binding force and $\gamma\dddot{\vec{r}}$ the radiative force. This radiative reaction force is the Abraham-Lorentz force of the radiated field upon the radiating charge. Its presence is of particular importance in resonance phenomena as will be shown below.

The electric field at the position of the charge in space is a function of time alone, thus the equation of motion becomes: $\ddot{\vec{r}} - \gamma\dddot{\vec{r}} + \omega_o^2\vec{r} = (e\vec{E}_o/m)e^{-i\omega t}$; where $\omega_o^2 = k/m$ is proportional to the binding energy of the charge. The solution of this equation is: $\vec{r} = [(e\vec{E}_o/m)e^{-i\omega t}]/[\omega_o^2 - \omega^2 - i\omega^2\gamma]$ At resonance ($\omega = \omega_o$), the radiative reactive term prevents the amplitude of oscillations from becoming unbounded by converting the energy of oscillation into radiant energy.

For the two gamma rays from Co^{60} used in this experiment there are no levels with energy spacing close enough to the energies of the incident gamma rays for the radiative effects to be important; thus the radiative term will be neglected. The displacement under these conditions is given by the following equation: $\vec{r} = (e\vec{E}_o/m)e^{-i\omega t}/(\omega_o^2 - \omega^2)$.

For the unbound case, it was also shown that dipole

radiation was the primary multipole contribution to the scattering, and that the differential cross section for this process is proportional to $(\hat{E}_I \cdot \vec{\vec{r}})^2/E_o^2$. Thus: $a \sim (\hat{E}_I \cdot \vec{\vec{r}})/E_o$; and in particular $a^{NF} \sim \omega^2/(\omega_o^2 - \omega^2)$, and $a^F \sim -\omega^2/\omega_o^2 - \omega^2)$.

Thus the non-relativistic amplitude for the scattering of electromagnetic radiation by a bound charge is given by: $a(^{NF}_{F}) \sim \pm \omega^2/(\omega_o^2 - \omega^2)$, where ω is the energy of the incident radiation and ω_o is the binding energy of the charge.

As mentioned earlier, in addition to single particle resonances, Giant Dipole Resonance can occur. Giant Dipole Resonance occurs for $E_\gamma \sim 15$ MeV ($\omega_o \sim 15$ MeV). Thus, for 1 MeV gamma rays ($\omega \sim 1$ MeV), one is observing the low energy tail end of this process ($\omega \ll \omega_o$). For this case $a_{NF} > 0$, and thus is 180° out of phase with the Nuclear Thomson amplitude.

Levinger[5] in 1951 has calculated the differential cross section for the Giant Dipole Resonance for $\omega \ll \omega_o$:

$$d\sigma/d\Omega = (Z^2e^2/Am_pc^2)^2[(1+\cos^2\theta)/2](N/Z)^2\left(\frac{\omega}{\omega_o}\right)^4(1+.8x)^2$$

The parameter $x (x < 1)$ has to do with an attractive neutron-proton exchange force and is about 1/2 for lead at $E_\gamma = 2{,}62$ MeV and is considerably smaller at $E_\gamma = 1.33$ MeV.

In 1954 Gell-Mann, Goldberger and Thirring[1] derived a similar expression for the special case of zero angle scattering using dispersion relations. The only difference had to do with the term x in Levinger's result. They obtained $1 + .1(A^2/NZ)$, instead of $1 + .8x$, making no assumptions about nuclear forces, showing no energy dependence and including very clearly all multiples of A, N, and Z. For

lead, Levinger's result is 1.4 at E_γ = 2.62 MeV and Gell-Mann, Goldberger and Thirring's result is 1.42 showing good agreement. However, for smaller E_γ, Levinger's results get smaller whereas Gell-Mann et al. stay the same. This discrepancy, however, is avoided since, as is shown below, the Giant Dipole effect is negligible as compared with the Nuclear Thomson effect.

Table 3 shows the ratio N/Z for the target elements used in this experiment.

Table 3

Element	N/Z	Abundance in %
Sn	66/50	14
	68/50	24
	70/50	32
Hg	120/80	23
	121/80	13
	122/80	30
Pb	124/82	26
	125/82	21
	126/82	52

The ratio of the Nuclear Resonance cross section to the Nuclear Thomson cross section is:

$$[(d\sigma/d\Omega)_{NR}/(d\sigma/d\Omega)_{NT}] = (N/Z)^2(\omega/\omega_o)^4[1 + .1(A^2/NZ)]^2$$

For E_γ = 1.33 MeV, A = 208, N = 126, and Z = 82 this ratio is $4.75(10^{-4})$. Since the cross section is proportional to the square of the amplitude, it is expected that the Nuclear Resonance amplitude is about 2% of the Nuclear Thomson amplitude.

The scattering amplitude for these two processes is given by:

$$a^2 = |a_{NT} - a_{NR}|^2 \quad \text{(since } a_{NT} < 0, \text{ and } a_{NR} > 0),$$

$$= |a_{NT}|^2 (1 - 2(\omega/\omega_o)^2 (N/Z)[1 + .1(A^2/NZ)])$$

$$= |a_{NT}|^2 (.95) \text{ for } E_\gamma = 1.33 \text{ MeV, A = 208, N = 126,}$$

and Z = 82. Thus, $|a_{NR}| \simeq .025\ |a_{NT}|$ and will be subsequently neglected.

Rayleigh Scattering

Rayleigh scattering is the major contributor to elastic scattering for energies below about 3 MeV; however, it is the least well accounted for theoretically.

Classically, the atom is set into oscillation by the incident electromagnetic radiation. In this case, one might well divide the total scattering into a nuclear contribution and an electron contribution. The nuclear part has already been discussed. The total electron contribution is the coherent sum of the contributions of each individual electron, taking into account binding and any interference effects.

The momentum supplied by the nucleus to the photon is given by: $\vec{q} = 2\vec{k}\sin\theta/2$, where $\vec{k}$ is the momentum of the incident gamma ray and θ is the scattering angle. Using this $\vec{q}$ one can investigate just how elastic Rayleigh scattering is. The least elastic scattering occurs for the lightest atom, which for the present experiment is tin. If momentum, $\vec{q}$, is transferred to the tin atom when the shift in energy of the scattered gamma ray is

$$\Delta E_\gamma = q^2/2m_{Sn}$$
$$= 4(E_\gamma/c)^2(\sin^2\theta/2)/2m_{Sn}$$
$$= 2(E_\gamma^2/m_{Sn}c^2)\ (\sin^2\theta/2)$$

The maximum ΔE_γ is for backscattering ($\theta = 180°$). For the case E_γ = 1 MeV we have: ΔE_γ = 20 eV. Thus, the shift in E_γ is not detectable by present state of the art detectors (see page 64).

In the section on Nuclear Resonance scattering, it

was shown that the scattering amplitude for dipole radiation including binding is given by: $a^{NF} \sim \omega^2/(\omega_o^2 - \omega^2)$. For Rayleigh scattering ω_o is about: 89 keV for lead, 85 keV for mercury, and 33 keV for tin; whereas ω is about 1 MeV for the gamma radiation used in this experiment. Thus, classically one expects $a_R^{NF} < 0$.

For this experiment $E_\gamma \sim 1$ MeV and $E_{ionization} \sim 90$ keV, thus, one might expect that any large momentum transfers would most likely ionize the atom. Therefore, elastic scattering should decrease as the scattering angle increases. Qualitatively, one could write for the Rayleigh scattering amplitudes:

$$a_R^{NF} = a_{NT}^{NF}[F(q)], \text{ and}$$

$$a_R^{F} = a_{NT}^{F}[F(q)], \text{ where } a_{NT}^{NF} \text{ is the nuclear Thomson}$$

amplitude with no polarization change, a_{NT}^{F} is the amplitude with polarization change, and F(q), the atomic form factor, is some forward peaked function of the momentum transfer, taking into account interference between the individual electron contributions.

In 1935, Franz[9] used as the form factor:

$F(q) = \int \psi^* \psi \, [m_e c^2/(E + Ze/r)] e^{i\vec{q}\cdot\vec{r}} d^3r$. He used non-relativistic Coulomb wavefunctions and expanded the bracketed term in powers of $Z\alpha$ keeping only the zeroth order term, i.e., $F(q) = m_e c^2 \int \psi^* \psi \, e^{i\vec{q}\cdot\vec{r}} d^3r$. His reasoning was as follows: as the incident gamma ray energy increases the effects of binding decrease with the consequence that the

factors multiplying higher powers of $Z\alpha$ decrease. He replaced $\psi^*\psi$ by ρ/e, the atomic charge density divided by the electron charge and used the Thomas-Fermi model of the atom to obtain ρ. In general, his results are good for $E_\gamma \leq m_e c^2$.

Brown, Peierls and Woodward[10] have shown that this basic assumption about the decreasing effects of binding as E_γ increases is misleading, and leads to incorrect results for $E_\gamma \sim 2m_e c^2$. They show that the relative importance of the binding increases rapidly with energy and interpret this in the following way:

> "The momentum transferred to the photon must be supplied by the nucleus through its coulomb field. In zero-order term this proceeds through the coulomb forces which act while the electron is in the ground state. In the higher-order terms, this momentum balance is mainly transferred to the nucleus between absorption and re-emission (or vise versa) of the photon. The transfer of a large amount of momentum is easier when the electron has a large momentum, as in the latter case, than when it is slow, as in the former."

Their method was as follows: They started with the same F(q) as Franz had used; however, they took the potential, Ze/r, into account exactly by using relativistic coulomb wavefunctions which are eigenfunctions of the unperturbed (no incident electromagnetic field) wave equation including binding and then expanded only in the effects of coupling with the transverse radiation field, i.e., in powers of α only. This, by the way, is essentially what one does by using Feynman diagrams and formalism.

They, however, take into account only the K shell electrons as they estimate its contribution to be 80% of the

Rayleigh cross section for momentum transfers greater than the characteristic K electron momentum: $q > Zm_e c$. They also show that L shell contributions are about 1/8 of the K shell contribution.

The differential cross section they obtain for the scattering of unpolarized gamma rays by the K shell electrons is given by: $\frac{d\sigma}{d\Omega} = R_o^2 (|M_{NF}|^2 + |M_F|^2)$, where R_o is the classical electron radius, and the matrix elements, M are given by the following equation:

$$M = (\hat{E}_I \cdot \hat{E}_S) \int \psi^* \psi \, (m_e c^2/(E + Ze/r)) e^{i\vec{q}\cdot\vec{r}} d^3r.$$

For states of circularly polarized light the individual matrix elements are given by:

$$M_{NF} = -[(1 + \cos\theta)/2] \int \psi^* \psi \, [m_e c^2/(E + Ze/r)] e^{i\vec{q}\cdot\vec{r}} d^3r$$

and

$$M_F = [(1 - \cos\theta)/2] \int \psi^* \psi \, [m_e c^2/(E + Ze/r)] e^{i\vec{q}\cdot\vec{r}} d^3r.$$

One check Brown, Peierls, and Woodward made on their amplitudes was to calculate the total photoelectron cross section from the optical theorem and then to compare their result with the known experimental value. Their results were within the experimental errors.

The computer calculated results for the matrix elements are given in Tables 4, 5, and 6 for 1.308 MeV, .654 MeV, and .327 MeV gamma rays on mercury.

We should in particular note three things about these calculated amplitudes:

(1) they are for mercury (Z = 80) only

(2) they are for E_γ = 1.308 MeV, .654 MeV, and .327 MeV gamma rays only

(3) they include contributions for the K shell electrons only

Table 4

E_γ = 1.308 MeV

θ	a^{NF} (R_o)	a^{F} (R_o)
0	-1.6989 + .0474i	0
15	- .9693 + .0315i	.0233 - .0040i
30	- .2905 + .0133i	.0374 - .0078i
45	- .0740 + .0086i	.0341 - .0068i
60	- .0133 + .0070i	.0293 - .0051i
75	.0025 + .0060i	.0254 - .0040i
90	.0062 + .0044i	.0233 - .0029i
105	.0053 + .0034i	.0224 - .0027i
120	.0038 + .0023i	.0215 - .0024i
135	.0023 + .0010i	.0218 - .0024i
150	.0011 + .0007i	.0217 - .0022i
165	.0009 + .0004i	.0209 - .0020i
180	0	.0206 - .0023i

(where R_o is the classical electron radius)

Table 5

E_γ = .654 MeV

θ	$a^{NF}(R_o)$	$a^{F}(R_o)$
0	- 1.7454	0
15	- 1.4713	.0329
30	- .9315	.0913
45	- .5044	.1264
60	- .2540	.1373
75	- .1227	.1357
90	- .0582	.1281
105	- .0265	.1194
120	- .0117	.1124
135	- .0045	.1062
150	- .0023	.1017
165	- .0009	.1018
180	- 0	.1029

(where R_o is the classical electron radius)

Table 6

E_γ = .327 MeV

θ	a^{NF} (R_o)	a^{F} (R_o)
0	- 1.83	0.0
15	- 1.70	.03
30	- 1.47	.12
45	- 1.15	.21
60	- .80	.32
75	- .52	.39
90	- .32	.44
105	- .20	.46
120	- .10	.48
135	- .05	.49
150	- .02	.49
165	- .008	.48
180	- 0.0	.46

(where R_o is the classical electron radius)

Since the scattering amplitude for lead and tin, in addition to mercury, at energies E_γ = 1.173 MeV and E_γ = 1.332 MeV is needed, an attempt will be made to correct for (1) and (2).

From Brenner, Brown and Woodward's[11] calculations, there is an approximate energy and Z dependence on the amplitude as is given by: $M \sim Z^n e^E$, where n is a function of the momentum transfer.

Anand and Sood[12] have experimentally investigated the n dependence of the momentum transfer. Table 7 lists the n dependence of the momentum transfer taken from graphs in their paper.

Table 7

Θ	15	20	30	45	60	75	90	105	120
n E_γ=1.17 MeV	1.4	1.68	2.2	2.5	2.68	2.73	2.7	2.68	2.65
n E_γ=1.31 MeV	1.5	1.9	2.33	2.6	2.7	2.73	2.68	2.65	-
n E_γ=1.33 MeV	1.5	1.9	2.33	2.6	2.7	2.73	2.68	2.65	-

Using this data one can extrapolate data at the same energy to any scatterer (any Z), ie: $M_N=(Z_N/Z_{Hg})^n M_{Hg}$. Table 8 gives the ratio $(Z_N/Z_{Hg})^n$, where $\beta_1=(Z_{Pb}/Z_{Hg})^n$, and $\beta_2=(Z_{Sn}/Z_{Hg})^n$.

Table 8

E_γ	θ	15	20	30	45	60	75	90	105	120	Avg.
1.31 & 1.33 MeV	β_1	1.04	1.05	1.05	1.07	1.07	1.07	1.07	1.07	-	1.06
	β_2	.49	.41	.33	.29	.28	.28	.28	.29	-	.33
1.17 MeV	β_1	1.03	1.04	1.05	1.06	1.07	1.07	1.07	1.07	1.07	1.06
	β_2	.52	.46	.36	.31	.29	.28	.28	.29	.29	.34

Thus one can calculate the effect for different Z provided one first corrects for the energy variation. Earlier it was mentioned, that the matrix elements are proportional to $Z^n e^{E_\gamma}$; thus, a plot of ln(M) vs E_γ at constant angle and Z is approximately linear, and extrapolation to other gamma ray energies is possible. The results of this extrapolation are given in Tables 9 and 10.

Table 9

Rayleigh Amplitudes for E_γ = 1.173 Mev

ϕ	Mercury		Lead		Tin	
	$a^{NF}(R_o)$	$a^{F}(R_0)$	$a^{NF}(R_0)$	$a^{F}(R_0)$	$a^{NF}(R_0)$	$a^{F}(R_0)$
0	-1.680+.0240i	0	-1.780+.2544i	0	-.8736+.0125i	0
15	-1.080+.0166i	.0263-.0021i	-1.145+.0176i	.0279-.0022i	-.5616+.0086i	.0137-.0011i
30	-0.386+.0070i	.0475-.0041i	-0.409+.0074i	.0504-.0043i	-.1390+.0025i	.0171-.0015i
45	-0.116+.0045i	.0460-.0036i	-0.123+.0048i	.0488-.0038i	-.0360+.0014i	.0143-.0011i
60	-.0275+.0037i	.0405-.0027i	-.0292+.0039i	.0429-.0029i	-.0080+.0011i	.0117-.0008i
75	.0000+.0032i	.0395-.0021i	.0000+.0034i	.0419-.0022i	.0000+.0009i	.0011-.0006i
90	.0038+.0023i	.0315-.0015i	.0040+.0024i	.0334-.0016i	.0011+.0006i	.0088-.0004i
105	.0055+.0018i	.0295-.0014i	.0058+.0019i	.0313-.0015i	.0016+.0005i	.0086-.0004i
120	.0005+.0012i	.0280-.0013i	.0005+.0013i	.0297-.0014i	.0001+.0003i	.0081-.0004i
135	.0008+.0005i	.0271-.0013i	.0008+.0005i	.0287-.0014i	.0002+.0001i	.0079-.0004i
150	.0004+.0004i	.0270-.0012i	.0004+.0004i	.0286-.0013i	.0001+.0001i	.0078-.0003i
165	.0005+.0002i	.0264-.0011i	.0005+.0002i	.0282-.0012i	.0001+.0001i	.0077-.0003i
180	0	.0265-.0012i	0	.0281-.0013i	0	.0077-.0003i

(where R_o is the classical electron radius)

Table 10

Rayleigh Amplitudes for E_γ = 1.332 MeV

θ	Mercury		Lead		Tin	
	a^{NF} (R_o)	a^{F} (R_o)	a^{NF} (R_o)	a^{F} (R_o)	a^{NF} (R_o)	a^{F} (R_o)
0	-1.6400+.0678i	0	-1.7380+.0719i	0	-.8036+.0322i	0
15	-0.9900+.0480i	.0253-.0057i	-1.0490+.0509i	.0282-.0060i	-.4851+.0235i	.0124-.0028i
30	-0.2990+.0190i	.0340-.01121	-0.3169+.0201i	.0413-.0119i	-.0987+.0062i	.0129-.0037i
45	-0.0740+.0123i	.0345-.0047i	-0.0784+.0130i	.0366-.0103i	-.0215+.0036i	.0100-.0028i
60	-0.0140+.0100i	.0275-.0073i	-0.0148+.0106i	.0292-.0077i	-.0039+.0028i	.0077-.0020i
75	0.0025+.0086i	.0262-.0057i	-0.0027+.0091i	.0278-.0060i	.0007+.0024i	.0073-.0016i
90	0.0062+.0063i	.0195-.0041i	0.0066+.0067i	.0207-.0043i	.0017+.0017i	.0055-.0011i
105	0.0053+.0049i	.0180-.0039i	0.0056+.0052i	.0191-.0041i	.0015+.0014i	.0052-.0011i
120	0.0042+.0033i	.0168-.0034i	0.0045+.0035i	.0178-.0036i	.0012+.0010i	.0049-.0010i
135	0.0025+.0014i	.0160-.0034i	0.0027+.0015i	.0170-.0036i	.0007+.0004i	.0046-.0010i
150	0.0012+.0010i	.0160-.0031i	0.0013+.0011i	.0170-.0033i	.0003+.0003i	.0046-.0009i
165	0.0010+.0006i	.0155-.0029i	0.0011+.0006i	.0164-.0031i	.0003+.0002i	.0045-.0008i
180	0	.0160-.0033i	0	.0170-.0035i	0	.0046-.0010i

(where R_o is the classical electron radius)

Delbruck Scattering

Classically, there is no analog to Delbruck scattering because one assumes the principle of linear superposition of electric fields and thus, from the beginning, rules out the possible interaction between two fields.

The complete angular and energy dependence of this effect has not been calculated because the integrals are too difficult; however, there have been several calculations of limited validity made.

The first important effort was that of Rohrlich and Gluckstern[3]. They evaluated the amplitudes for forward scattering ($\theta = 0°$); first, by using Feynman diagrams and formalism, and then by using dispersion relations, as outlined earlier in the section on the phases of the scattering amplitudes, and approximating the total scattering cross section by the well known cross section for pair production.

In addition to their effort there are two other calculations relevant to the experimentalist. One by Herrera and Roman[13] (for $E_\gamma < 2m_e c^2$, all Z, and all θ), and the other by Ehlotzky and Sheppey[14] (for 1 MeV$< E_\gamma <$ 20 MeV, all Z, and $10° \leq \theta \leq 120°$).

Herrera and Roman have calculated the differential cross section by evaluating a transition matrix connecting the initial and final state of the electromagnetic field; ie: $d\sigma/d\Omega \sim |M_{fi}|^2$, where $M_{fi} = \langle \psi_f | L_I | \psi_i \rangle$, and L_I is an effective classical interaction Lagrangian. The term L_I is

a function of the two basic invariants of the electromagnetic field: $L_I \sim \int (4I_1^2 + 7I_2^2)d^4x$, where $I_1 = (1/2)(H^2 - E^2)$ and $I_2 = \vec{E}\cdot\vec{H}$. They then proceeded to quantize the fields, in the usual manner of quantum electrodynamics, so that the interaction Lagrangian would be able to create and destroy photons even for gamma ray energies below the threshold for electron pair production. Including only terms which were quadratic in the fields, in L_I, was required so as to be consistent with the Feynman diagrams for Delbruck scattering. A divergent term, which appeared in M_{fi}, was reasoned to mean that their semi-classical calculation was valid below some cut-off energy. They evaluated this cut-off energy by calculating M_{fi} and then requiring their result to reduce to the result of Rohrlich and Gluckstern at zero degrees scattering angle. This fixed the cut-off at $1.92\ m_e c^2$, or just below electron pair production energies.

They obtained for the differential cross section:

$d\sigma/d\Omega = KZ^4E_\gamma^4[101\cos^2\theta + 40\cos\theta + 101]$

$= KZ^4E_\gamma^4[(202(1 + \cos^2\theta)/2) + 40\cos\theta]$, where K is a constant. The term $(1 + \cos^2\theta)/2$ is just the term one would expect classicly from an electric dipole radiator of order $l = m = 1$. The other term, proportional to $\cos\theta$, can be thought of as due to a magnetic dipole radiator of order $l = m = 1$. Thus, one can view the Delbruck effect, for $E_\gamma < 1.92\ m_e c^2$, to be the superposition of electric and magnetic dipole radiation fields, linearly polarized and 90° out of phase[10].

Since the energies of the gamma rays used in this experiment are greater than 2 $m_e c^2$, Herrera and Roman's calculation can not be applied to the results reported here. However, their conclusions as to the polarization of the scattered radiation may be valid even for the energy range investigated in this experiment. Thus, a polarization measurement may help distinguish the Delbruck process from the other coherent processes.

Ehlotzky and Sheppey used Kessler's[15] expressions for the imaginary part of the Delbruck scattering amplitude and Cauchy's principle value integral (dispersion relation) to obtain the real part of the Delbruck scattering amplitude. The integrals are calculated by computer, and an accuracy of 5 to 10 % is claimed.

Their results are given in Table 11. The amplitudes listed are those for polarization (1) parallel and (2) perpendicular to the scattering plane (plane formed by $\vec{k}_I$ and $\vec{k}_S$).

Table 11

Results of Ehlotzky and Sheppey for E_γ = 1.329 MeV

θ	$a_1[(\alpha Z)^2 R_o]$		$a_2[(\alpha Z)^2 R_o]$	
	$a_{1\parallel}$	$a_{1\perp}$	$a_{2\parallel}$	$a_{2\perp}$
10	.073	.058	.0056	.0055
20	.045	.029	.0051	.0040
30	.030	.015	.0044	.0039
45	.018	.0054	.0034	.0024
60	.0117	.0005	.0026	.0011
90	.0068	-.0028	.0019	-.00068
120	.0051	-.0040	.0018	-.0015

Where $a_\parallel$ is the amplitude for parallel polarization, and $a_\perp$

is the amplitude for perpendicular polarization. The subscripts 1 and 2 represent the real and imaginary parts of the scattering amplitude respectively, and the constant R_o is the classical electron radius.

Conversion to the two states of circular polarization will be made so as to be consistent with the calculations of the other coherent processes.

In the section on Nuclear Thomson scattering it was shown that the scattering amplitude is proportional to $\hat{E}_I \cdot \hat{E}_S$. For linear polarization before and after scattering $\hat{E}_I \cdot \hat{E}_S = \cos\theta$ for the polarization components parallel to the scattering plane and $\hat{E}_I \cdot \hat{E}_S = 1$ for the polarization components perpendicular to the scattering plane. To see this, a diagram is drawn below for both the incident and scattered radiation; indicating in particular, the polarization components parallel and perpendicular to the scattering plane.

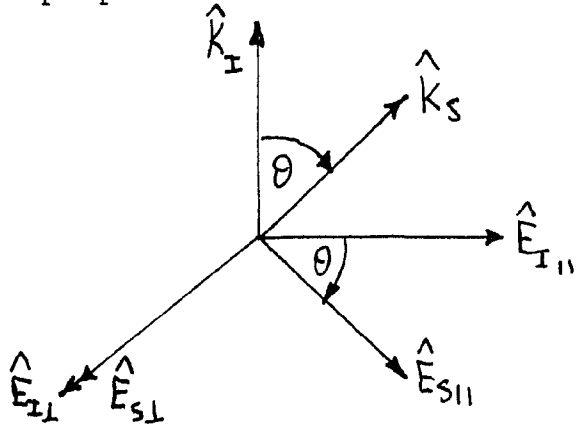

The amplitude for no polarization change, derived earlier for the special case of circularly polarized light, is given by: $a^{NF} \sim -(1 + \cos\theta)/2$, while for no polarization change $a^F \sim (1 - \cos\theta)/2$. Thus, it is easy to see that defining $a^{NF} \sim -(a_\perp + a_{\parallel})/2$, and $a^F \sim (a_\perp - a_{\parallel})/2$, produces the

proper flip and no-flip amplitudes. Table 12 gives the amplitudes for flip and no-flip for lead, mercury and tin.

Extrapolation to other E_γ and Z can be accomplished since $a_{Del} \sim (ZE_\gamma)^2$. The results of extrapolating the data in Table 12 to energies 1.17 MeV and 1.33 Mev is presented in Tables 13 and 14.

Table 12

Delbruck Flip and No-Flip Amplitudes for E_γ= 1.329 MeV

	Mercury		Lead		Tin	
θ	a^{NF} (R_o)	a^{F} (R_o)	a^{NF} (R_o)	a^{F} (R_o)	a^{NF} (R_o)	a^{F} (R_o)
10	.0023+.0019i	.0026+.00020i	.0734+.00200i	.0027+.00002i	.0086+.00070i	.0001+.00007i
20	.0126+.0017i	.0027+.00003i	.0132+.00180i	.0028+.00003i	.0049+.00070i	.0010+.00001i
30	.0077+.0017i	.0026+.00010i	.0081+.00180i	.0027+.00010i	.0030+.00070i	.0010+.00003i
45	.0040+.0010i	.0021+.00020i	.0042+.00110i	.0022+.00020i	.0016+.00040i	.0008+.00006i
60	.0021+.0006i	.0019+.00030i	.0022+.00060i	.0020+.00030i	.0008+.00025i	.0007+.00010i
90	.0007+.0002i	.0016+.00040i	.0007+.00020i	.0017+.00040i	.0003+.00008i	.0006+.00017i
120	.0002+.0002i	.0016+.00060i	.0002+.00005i	.0017+.00060i	.0007+.00002i	.0006+.00020i

(where R_o is the classical electron radius)

Table 13

Delbruck Amplitudes for E_γ = 1.17 MeV

θ	Mercury		Lead		Tin	
	a^{NF} (R_o)	a^{F} (R_o)	a^{NF} (R_o)	a^{F} (R_o)	a^{NF} (R_o)	a^{F} (R_o)
30	.0059+.00130i	.0020+.0007i	.0062+.00140i	.0021+.0001i	.0023+.0005i	.0008+.0000i
45	.0031+.00080i	.0016+.0002i	.0032+.00080i	.0019+.0002i	.0012+.0003i	.0006+.0001i
60	.0016+.00050i	.0015+.0002i	.0017+.00050i	.0015+.0002i	.0006+.0002i	.0006+.0001i
75	.0009+.00030i	.0013+.0003i	.0009+.00030i	.0014+.0003i	.0004+.0002i	.0005+.0001i
90	.0005+.00020i	.0012+.0003i	.0005+.00020i	.0013+.0003i	.0002+.0001i	.0005+.0001i
105	.0003+.00030i	.0012+.0004i	.0003+.00010i	.0013+.0004i	.0001+.0001i	.0005+.0002i
120	.0002+.00004i	.0012+.0005i	.0002+.00004i	.0013+.0005i	.0001+.0000i	.0005+.0002i

(where R_o is the classical electron radius)

Table 14

Delbruck Amplitudes for E_γ= 1.33 MeV

θ	Mercury		Lead		Tin	
	a^{NF} (R_o)	a^{F} (R_o)	a^{NF} (R_o)	a^{F} (R_o)	a^{NF} (R_o)	a^{F} (R_o)
30	.0076+.00170i	.0026+.0001i	.0080+.00180i	.0027+.0001i	.0030+.0007i	.0010+.0000i
45	.0040+.00100i	.0021+.0002i	.0042+.00110i	.0022+.0002i	.0016+.0004i	.0008+.0000i
60	.0021+.00060i	.0019+.0003i	.0027+.00060i	.0020+.0003i	.0008+.0002i	.0007+.0001i
75	.0012+.00030i	.0017+.0003i	.0012+.00040i	.0019+.0003i	.0005+.0002i	.0006+.0002i
90	.0007+.00020i	.0016+.0004i	.0007+.00020i	.0017+.0004i	.0003+.0001i	.0006+.0002i
105	.0004+.00030i	.0016+.0005i	.0004+.00010i	.0017+.0005i	.0002+.0001i	.0006+.0002i
120	.0002+.00005i	.0016+.0006i	.0002+.00005i	.0017+.0006i	.0001+.0000i	.0006+.0002i

(where R_o is the classical electron radius)

Appendix

Number

1 Gell-Mann, Goldberger, and Thirring, Phys. Rev., 95, 1612 (9/54)

2 Erber, Ann. Phys., 6, 319 (1959)

3 Rohrlich and Gluckstern, Phys. Rev., 86, 10 (1952)

4 Levinger and Rustgi, Phys. Rev., 103, 439 (7/56)

5 Levinger, Phys. Rev., 84, 523 (11/51)

6 Jackson, "Classical Electrodynamics", Chapter 16

7 Landau and Lifshitz, "Classical Theory of Fields", Chapter 9

8 Jackson, "Classical Electrodynamics", Chapter 17

9 Franz, Z. Physik, 98, 314 (1936)

10 Brown, Peirels, and Woodward, Proc. Roy. Soc. (Lon.), A227, 51 (1954)

11 Brenner, Brown and Woodward, Proc. Roy. Soc. (Lon.). A227, 59 (1951)

12 Anand and Sood, Nucl. Phys., 73, 368 (1965)

13 Herrera and Roman, Nuovo Cim., 33, 1657 (9/64)

14 Ehlotzky and Sheppy, Nuovo Cim., 33, 1185 (1964)

15 Kessler, Jour. Phys. Rad., 19, 739 (1958)

Review of Other Experiments

In 1958, Bernstein and Mann[1] used a NaI(Tl) detector to detect gamma radiation (from a 100 mCi Co^{60} source), scattered by rings of lead, uranium and tin. Since they were unable to resolve the elastic scattering from the inelastic background, analysis was quite difficult.

In 1967, Dixon and Storey[2] irradiated sheets of lead (with cross sectional area of 25 $in.^2$ and thickness ranging from 1/4 to 1/2 inch) with gamma rays from a 100 Ci Co^{60} source and used a 1 cm^3 GeLi detector (with resolution of about 6 keV for Co^{60} gamma rays) to detect the scattered radiation.

In 1970, Hardie, Merrow, and Schwandt[3] using a GeLi detector (with an active volume of 12 cm^3 and a resolution of 3.6 keV for Co^{60} gamma rays) measured the cross section for angles between 60° and 135° using the same geometry as Dixon and Storey, in order to improve the statistical accuracy of the measurements. It was later decided to complete the measurements by including the angular range from 12° to 60°. This was completed in 1971 by Hardie, DeVries, and Chiang[4].

In 1970, Basavaraju and Kane[5] investigated the scattering of Co^{60} gamma radiation by mercury and various other elements for scattering angles of 90° and 124.5°. They used a 1 Ci Co^{60} source and a NaI(Tl) detector.

Tables 15 to 20 summarize the existing data for the

scattering of Co^{60} gamma rays from lead, tin, and mercury.

In addition to these experiments which have in part tried to establish the real part of the Delbruck scattering amplitude, there have been two other experiments done at high energy which have tried to establish the imaginary part of the amplitude.

The first was done in 1960 by Moffat and Stringfellow[6], in which gamma radiation with mean energy of 87 MeV (produced by bremsstrahlung in a synchrotron) was scattered from lead, uranium, tungsten, silver, and aluminum. Their results suggested the existence of the imaginary part of the Delbruck scattering amplitude, although they had difficulty resolving the elastic spectrum from the inelastic contribution.

In 1969, Jackson and Wetzel[7] scattered 10.8 MeV gamma radiation (produced by reactor activation of a nitrogen compound) from lead and uranium. For this energy region they argue that Rayleigh scattering can be neglected compared to Giant Dipole scattering and Delbruck scattering. Since the differential cross section for Giant Dipole scattering is symetric about 90°, any forward peaking of the cross section is attributed to Delbruck scattering. Their results showed a definite increase in scattering for angles less than 75°, thus establishing the imaginary part of the Delbruck scattering amplitude.

Table 15

$d\sigma/d\Omega$ (mb/st. rad.) for the Elastic Scattering of 1.17 MeV Photons from Lead

θ	Present Results	Dixon and Storey[2]
10	423. ± 25.	
20	75.3 ± 6.0	
30	33.1 ± 1.7	13.0 ± 1.0
40	5.33 ± .43	
45		1.91 ± .10
50	1.17 ± .12	
60	.517 ± .083	.350 ± .026
70	.336 ± .047	
75		.246 ± .017
80	.242 ± .012	
90	.204 ± .037	.199 ± .009
100	.154 ± .022	
105		.161 ± .010
110	.145 ± .025	
120	.117 ± .029	.150 ± .007
130	.145 ± .026	
140	.197 ± .053	
150		.150 ± .015

Table 16

$d\sigma/d\Omega$ (mb/st. rad.) for the Elastic Scattering of 1.33 MeV Photons from Lead

θ	Present Results	Hardie et. al.[3,4]	Dixon et. al.[2]	Bernstein et. al.[1]
10	237. ±13.8			
12		121.6 ±7.2		
15				133. ±22.
20	36.67 ± 2.93	32.1 ±1.9		
30	10.5 ± .8	7.17 ± .37	6.20 ±.40	10. ± 1.5
40	2.54 ± .30			
45		.791± .042	.760±.040	1.5 ± .4
50	.298± .084			
60	.183± .053	.190± .010	.185±.013	.47 ± .12
70	.121± .034			
75		.125± .007	.118±.009	.24 ± .06
80	.104± .030			
90	.097± .031	.108± .006	.113±.007	.16 ± .05
100	.096± .021			
105		.095± .006	.099±.006	.12 ± .05
110	.090± .031			
120	.075± .019	.094± .006	.093±.006	
130	.077± .022			
135		.098± .006		
140	.130± .038			
150			.099±.012	

Table 17

$d\sigma/d\Omega$ (mb/st. rad.) for the Elastic Scattering of 1.17 MeV Photons from Mercury

θ	Present Results
10	319.5 ±24.6
20	54.2 ± 5.2
32	14.7 ± 1.2
40	5.69 ± .66
50	1.83 ± .29
60	.541 ± .212
70	.151 ± .047
80	.114 ± .034

Table 18

$d\sigma/d\Omega$ (mb/st. rad.) for the Elastic Scattering of 1.33 MeV Photons from Mercury

θ	Present Results	Basavaraju et. al.[5]
10	171.9 ±12.4	
20	23.6 ± 2.4	
32	3.91 ± .36	
40	1.76 ± .39	
50	.744 ± .223	
60	.198 ± .101	
70	.103 ± .033	
80	.081 ± .012	
90		.0980 ± .0091
125		.0825 ± .0010

Table 19

$d\sigma/d\Omega$ (mb/st. rad.) for the Elastic Scattering of 1.17 MeV Photons from Tin

θ	Present Results
10	67.7 ±6.4
20	26.4 ±4.0
30	9.10 ±1.00
40	2.57 ± .49
60	.202± .077
100	.039± .017

Table 20

$d\sigma/d\Omega$ (mb/st. rad.) for the Elastic Scattering of 1.33 MeV Photons from Tin

θ	Present Results	Bernstein et. al.[1]
10	39.3 ±4.3	
15		42. ±8.
20	14.0 ±2.0	
30	4.46 ± .09	1.3 ± .3
40	1.14 ± .35	
45		.21 ± .07
50	.199± .060	
60	.111± .041	.050± .02
75		.032± .015
90	.023± .016	
100	.020± .014	
105		.006± .006

Appendix

Number

1 Bernstein and Mann, Phys. Rev., 110, 805 (5/58)

2 Dixon and Storey, Can. Jour. Phys., 46, 1153 (1963)

3 Hardie, Merrow, and Schwandt, Phys. Rev., 1, 714 (2/70)

4 Hardie, DeVries, and Chiang, Phys. Rev., 3, 1287 (3/71)

5 Basavaraju and Kane, Nucl. Phys., A149, 49 (1970)

6 Moffat and Stringfellow, Proc. Roy. Soc. (Lon.), A254, 242 (1960)

7 Jackson and Wetzel, Phys. Rev. Lett., 22, 1008 (5/69)

THE EXPERIMENT IN BRIEF

As mentioned earlier, the four elastic processes can be studied by varying the energy of the incident gamma radiation, the Z of the scatterer, the angle of the scatter, and by measuring the degree of polarization of the scattered gamma rays.

In the work of this paper, the angular distributions of gamma radiation, from a Co^{60} scource, scattered by Pb, Hg, and Sn have been investigated. By "summing" over all scattered gamma rays the two polarization components present are ignored.

Ring geometry was used to maximize the count rate from a 25 mC Co^{60} source. Each set of data consisted of a ring-in, ring-out, efficiency and pileup sequence of measurements, for each of the scattering samples used.

The purpose of these studies is to measure the differential scattering cross section for Sn, Hg, and Pb at the two gamma ray energies- 1.173 MeV and 1.332 MeV; and further to compare these results with the theoretical cross sections, to the extent that they can be readily calculated.

Experimental Method

Introduction

Figure 1 shows the experimental arrangement. Ring geometry was chosen in order to maximize the count rate from a 25 mCi Co^{60} source. The source, whose active dimensions were 1 mm high by 1 mm in diameter, was used to irradiate various metalic rings.

The rings were made from lead, mercury and tin of greater than 99% purity. Scattered radiation was detected, using a 35 cm^3 GeLi crystal of approximately cylindrical geometry. The energy resolution of this detector for Co^{60} gamma radiation was 3.1 KeV F.W.H.M., with a peak to compton ratio of 20 to 1. A 24" long by 2" diameter cylindrical lead shield was placed between the source and detector in order to minimize direct irradiation of the detector as well as to promote multiple inelastic scattering events. The latter was desired in order to remove as much of the inelastic background from the vicinity of the elastic spectrum as was possible.

Figure 2 shows a block diagram of the electronics. After amplification and shaping, pulses were sent to a pileup rejector to increase resolution, degraded by the pileup of many low energy events, and then to a 4096 channel analyzer with digital stabilizing. The digital stabilizer minimizes conversion gain drift over long counting periods.

Apparatus

A 10' x 5' x 5' cage of aluminum Dexion was constructed to support the ring, source, shield and detector in various geometrical configurations. Lucite supports were machined for the source and rings to fix them in space.

The rings were formed into a circle of fixed radius by supporting them on large circular lucite spools machined to accept the metal rods. These forms were in turn slipped into and out of a lucite support suspended in the cage.

For the source, a cylindrical block of lucite was machined with a concentric hole of exact diameter as the stainless steel source container. The source was inserted into this form, which was placed into the source support suspended in the cage.

The reason the source and rings had both a form and support was due to the alignment technique to be discussed later.

The lead shield was fixed in space using two cylindrical lucite blocks with a concentric hole machined in each to accept the shield.

Each support was fixed to the cage using three piano wires. Figure 3 shows the system of support. The wire from each support was connected to a turnbuckle. The turnbuckle was then connected to a thumbscrew (see figure 4) which was mounted with bolts to the cage. Adjustment of the three turnbuckles and/or the three thumbscrews associated with

each support permitted three dimensional orientation of each object.

Alignment Technique

The ring, source, and detector were centered on and oriented perpendicular to a line in space, established through the use of a HeNe laser. Thin aluminum or bakelite discs were machined to fit into each of the lucite supports. At the center of each disc, a hole of .030" diameter was drilled. A 2" x 1-1/2" diameter tube was mounted flush to the disc and concentric with its center. Opposite ends of the tube were machined parallel (see figure 5). Across the free end of the tube, a glass slide with mirrored surface could be placed.

Thus, alignment was attained as follows:

1. a disc is placed in the appropriate support
2. the laser is turned on
3. using the three turnbuckles, the disc (and thus support) is centered on the beam
4. the mirrored slide is placed over the free end of the tube. The laser beam having been centered on the pinhole passes through the hole, hits the mirror and is reflected back.
5. orientation of the disc (and support) is then adjusted, using the three thumbscrews so that the reflected laser beam goes back out of the pinhole and back to the laser itself. When the reflected beam is coincident with the incident beam, alignment

is complete.

This technique, then, centers the disc on and perpendicular to the laser beam. The detector alignment was slightly different. First, the detector was scanned in three dimensions so as to locate the crystal in the head of the detector and to establish the active volume therein. A 1 mCi Co^{60} source was placed behind a slit formed by placing two 8" x 4" x 2" lead bricks together. This system was placed on the table of a milling machine which, having the facility of motion in three perpendicular planes, was ideal for such a scan.

A single channel analyzer with window centered on the 1.33 MeV gamma ray from Co^{60} sent pulses to a scaler for tabulation. Thus, a point by point plot of the detector geometry was established. The axis of the crystal was found to be approximately perpendicular to the front face of the detector locating the center front of the crystal.

The alignment of the detector is then accomplished by orienting the detector face perpendicular to and centered on the laser beam. This is done using the dot on the face of the detector as well as a mirrored slide placed across the face of the detector.

The alignment of the shield was done adequately by eye since all that is necessary is that the shield be roughly centered on the beam. Further, since the shield was not moved during an entire set of taking data, a slight misalignment would be subtracted out by the ring out run.

Additional considerations as to the position of the shield relative to the source, scatterer and detector are as follows:

1. placement and removal of rings from their support had to be possible without moving the shield
2. both the source and the detector had to have an unimpeded line of sight to the scattering ring
3. the shield was placed as close to the source as was possible in order to increase the scattering angle from the shield (this tends to shift the energy of the inelastically scattered Compton gamma rays to lower energy; thus improving the background in the vicinity of the elastically scattered gamma rays.

Therefore, the total alignment procedure was as follows:

1. align the detector on and perpendicular to the laser beam
2. align the source support
3. align the ring support
4. align the shield by eye

Measurement of the Scattering Angle

By measuring the distance from the detector to the ring (l_{rd}), the ring to the source (l_{rs}), as well as the diameter of the ring, it is easy to calculate the scattering angle (see figure 9).

The diameters of the rings are measured using vernier calipers. The distances l_{rs} and l_{rd} are measured by placing a meter stick between the different objects.

Measurement of the Detector Efficiency and Solid Angle Subtended from the Ring to the Detector

For each scattering configuration, the efficiency of the detector for observing 1 MeV gamma radiation coming from the ring has to be measured. This is established by placing a weak Co^{60} source of known yield at the position of the ring and measuring the count rate. The measured count rate is then given by: $R = R_o \epsilon \Delta\Omega/4\pi$ where R_o is the calibrated rate for the source and R is the measured rate. The ratio of R/R_o is the desired quantity. R_o was 1.02 μCi on April 12, 1967.

Source Calibration

The 25 mCi Co^{60} gamma ray source was calibrated by the National Bureau of Standards at Gaithsburg, Maryland, on December 24, 1969 and its activity was measured at 23.11 $\pm$ 3% mCi. The method of calibration was as follows:

a weak Co^{60} source was calibrated using the coincidence technique of measuring the singles rates as well as the coincidence rate. This calibrated source was then used to calibrate an ionization chamber. The ionization chamber in turn was used to measure the activity of our source.

The activity was previously measured by New England Nuclear, the company which produced the source, and they, using an ionization chamber, calibrated the source at $24.8 \pm 3\%$ mC on May 30, 1969. This measurement is equivalent to $22.95 \pm 3\%$ on December 24, 1969, the day of the National Bureau of Standards calibration. A comparison is made below:

On December 24, 1969:

1. N.E.N. $22.95 \pm .69$ mC
2. N.B.S. $23.11 \pm .69$ mC

Rings

The rings of metal were made from rods of 99.99% pure lead and tin. Quarter inch diameter and half inch diameter rods were used. From these, three different diameter rings were formed. From the 1/4" diameter rods, rings of 10.6 cm and 21.6 cm diameters were formed while a 45.2 cm diameter ring was formed from the 1/2" diameter rod.

The mercury rings were formed using plastic tubing of two different diameters placed onto the ring forms. A 1/4" outside diameter, with a 1/16" wall was used to make the 10.6 cm and 21.6 cm diameter rings while a 1/2" outside diameter with 1/16" wall was used to make the 45.2 cm

diameter ring. The mercury was then poured into the tubes while on the forms and stoppered up.

Thus, for each ring diameter, there were four different forms: one for the lead, one for the tin, one for the mercury and one blank.

Measurement of the Differential Cross Section

The differential cross section for elastic scattering measured in this experiment can be established by three counting measurements.

The number of monoenergetic gamma rays incident on the ring per unit time is given by N_I:

$$N_I = \frac{A'}{4\pi r^2} N_{os}$$

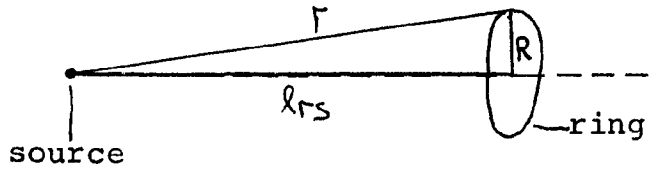

where A' is the area of the ring, r is the distance from the source to the ring and N_{os} is the number of monoenergetic gamma rays emitted by the source per unit time. Since one is interested in the number of elastically scattered gamma rays per unit solid angle, one has:

$$N_{IEL} = \frac{N \left(\frac{d\sigma}{d\Omega}\right)_{EL}}{A'} N_I$$

where $\left(\frac{d\sigma}{d\Omega}\right)_{EL}$ is the differential cross section for elastic scattering per atom and N is the number of atoms present. Thus:

$$N_{IEL} = \left[\frac{N \frac{d\sigma}{d\Omega}_{EL}}{4\pi(R^2+l_{rs}^2)}\right] N_{os}$$

Of these N_{IEL} elastically scattered gamma rays, the number registered in the detector is given by N_D:

$$N_D = N_{IEL}\, A\Omega_D \epsilon_s$$

where A is an attenuation factor (less than one) which determines the fraction of the elastically scattered gamma rays to escape the ring in the direction of the detector, Ω_D is the solid angle subtended at the ring by the detector and ϵ_s is the efficiency of the detector for registering these monoenergetic gamma rays.

For each scattering configuration, the efficiency of the detector has to be measured. This is established by placing a weak Co^{60} source of known yield at the position of the ring and measuring the count rate. The number of monoenergetic gamma rays detected per unit time is given by N_ϵ :

$$N_\epsilon = N_{o\epsilon} \frac{\Omega D}{4\pi} \epsilon_s$$

where $N_{o\epsilon}$ is the number of gamma rays emitted by the weak source per unit time, Ω_D is the solid angle subtended at the ring by the detector and ϵ_s is the efficiency. Thus, by making this measurement, we obtain both Ω_D and ϵ_s in $\left(\frac{d\sigma}{d\Omega}\right)_{EL}$:

$$\Omega_D \epsilon_s = \frac{N_\epsilon}{N_{o\epsilon}} 4\pi$$

Putting this into N_D we have:

$$N_D = \left[\frac{N\left(\frac{d\sigma}{d\Omega}\right)EL}{R^2 + l_{rs}^2}\right] N_{os} A \frac{N\epsilon}{N_{o\epsilon}}$$

However, less than N_D pulses reach the analyzer. This is not due to pileup at the analyzer but rather at the pileup rejector. The dead time in the analyzer due to pileup there is accounted for automatically by running in live-time mode. The dead time in the pileup rejector is not accounted for since the pileup rejector may be dead while the analyzer is live and waiting for pulses. To estimate this dead time, two different measurements were made. One was to utilize the natural K^{40} background present (E_γ =1.459 MeV). By comparing the K^{40} background with no source present, with the K^{40} background present during each elastic scattering measurement, one has a way of estimating the dead time in the pileup rejector. Also, by placing a weak Co^{60} source ($\sim$ 1 μCi) near the detector, and then alternately placing and then removing the 25 mCi Co^{60} source from the scattering position (with all other scattering components in Position), another estimate of the dead time can be made. The ratio of the no pileup run to the pileup run gives the pileup correction factor P ($P \geq 1$). It was found that these two different methods yielded values for P that were within 5% of one another. Better agreement is not to be expected due to the different nature of these two measurements. The weak source measurement yields a P which does not take into account count rate variations or electronic instabilities whereas the K^{40} measurement yields an average P which does account for changes in the rejector dead time during the run. This averaged pileup correction factor was used in the cross

section calculation (see Table 21).

Therefore, the number of pulses reaching the analyzer is N_S:

$$N_S = \frac{N_D}{P}$$

Solving for $\left.\frac{d\sigma}{d\Omega}\right)_{EL}$ one has:

$$\left.\frac{d\sigma}{d\Omega}\right)_{EL} = \left[\frac{N_S}{N_{OS}}\right]\left[\frac{N_{O\epsilon}}{N_\epsilon}\right]\left[\frac{R^2+l_{rs}^2}{N}\right]\left[\frac{P}{A}\right]$$

This is the formula used to calculate the elastic cross section and as mentioned in the beginning of this section, there are three counting measurements necessary: N_S, N_ϵ and P.

The distance R is measured by large calipers, l_{rs} is measured by placing a two meter stick between the source and ring (see figure 9), and N is measured by weighing each ring, dividing by the atomic weight, and multiplying by Avagadro's number (see Table 22).

The attenuation factor, A, is determined by the exponential term $e^{-\mu l}$ where μ is the linear attenuation coefficient for the particular scattering material being used and l is the distance traversed within the scatterer from entrance to the point of elastic scattering and then out. The factor μ is a function of the gamma ray energy and is obtained from interpolating tables.

Table 21

Pileup Correction Factor-P

Scatterer	Scat. Angle θ	l_{sd} (cm)	K^{40} (132c/m)	1 μCi Co^{60}
Lead & Tin	10	123.2	1.47	1.40
	19	122.6	1.47	1.46
	29	102.3	1.48	1.50
	40	102.3	1.51	1.52
	51	84.0	1.58	1.64
	61	86.0	1.66	1.64
	70	78.6	1.69	1.68
	81	72.3	1.65	1.68
	91	67.3	1.68	1.74
	101	62.9	1.66	1.70
	109	59.6	1.71	1.69
	121	69.2	1.66	1.69
	130	72.8	1.64	1.68
	140	84.4	1.55	1.53
Mercury	10	122.3	1.23	1.29
	20	122.3	1.22	1.22
	32	75.5	1.46	1.50
	40	75.5	1.38	1.43
	50	75.5	1.34	1.40
	60	75.5	1.30	1.35
	70	75.5	1.40	1.38
	80	75.5	1.39	1.40

Table 22

Number of Atoms In Scatterer

Element	Lead			Tin			Mercury		
Atomic Weight	207.19			118.69			200.59		
Ring	S	M	L	S	M	L	S	M	L
Weight in grams	119.2	239.2	2156	76.5	155.7	1396	33.34	70.79	1235
Number of atoms (10^{23})	3.46	6.95	62.7	3.88	7.90	70.81	1.0	2.13	37.1

The number of atoms present in the ring is given by: $N = (W/At.W.)Av.$, where W is the weight of the scatterer in grams, At. W. is the atomic weight of the scatterer in grams, and Av. is avagadro's number. The letter S, M, and L stand for small, medium, and large respectively.

The attenuation factor A is given by:

$$A = \left[\iint e^{-\mu\sqrt{x^2+y^2}}\, dx\,dy\right] \Big/ \left[\iint dx\,dy\right]$$

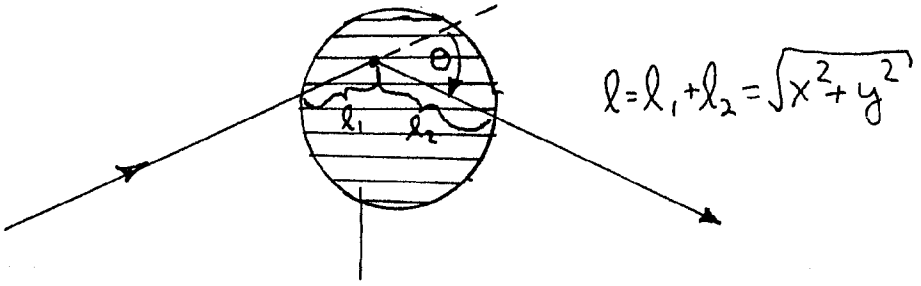

Cross Section of
the Scattering Ring

In general, the integral can not be solved exactly so it was evaluated for three particular scattering angles: 0°, 90°, and 180°. The variation in A was found to be less than 15% for scattering angles between 0° and 180°. For 0° and 180° the integrals can be solved exactly whereas for 90° a numerical integration was carried out. A check on this method was carried out by calculating A for 0° and 180° geometries and comparing with the exact results. The exact integrals are modified Struve functions (functions of Bessel functions).

The results for A are given in Table 23. Table 24 gives values for the modified Struve functions. Graph 1 gives mass attenuation coefficients- ϱ (cm^2/gm). To obtain the linear attenuation coefficients multiply by the density of the material.

Table 23

Table of Attenuation Coefficient - A

Material	Density	Linear Attenuation Coefficient	Attenuation Coefficient A		
	gm/cm^3	$\mu(cm^{-1})$	0°	90°	180°
Pb (s&m)	11.35	.70	.710	.717	.704
E_γ = 1.17 (lg)	11.35	.70	.508	.530	.522
E_γ = 1.33 (s&m)	11.35	.635	.732	.740	.726
(lg)	11.35	.635	.540	.561	.550
Hg (s&m)	13.546	.832	.815	.822	.806
E_γ = 1.17 (lg)	13.546	.832	.546	.566	.555
E_γ = 1.33 (s&m)	13.546	.755	.830	.838	.822
(lg)	13.546	.755	.576	.595	.581
Sn (s&m)	7.31	.387	.826	.834	.818
E_γ = 1.17 (lg)	7.31	.387	.684	.702	.681
E_γ = 1.33 (s&m)	7.31	.360	.837	.839	.828
(lg)	7.31	.360	.703	.721	.698

The letters s, m & lg stand for small ring, medium ring and large ring respectively.

The attenuation coefficient listed in the above table for 0° and 180° are given by the following equations:

$$A(0°) = 1 - [\pi/2][I_1(2\mu R) - L_1(2\mu R)]$$

$$A(180°) = [1/2\mu R][I_1(4\mu R) - L_1(4\mu R)]$$

Where μ is the linear attentuation coefficient, R is the cross sectional radius of the scatterer and the bracketed terms are the modified Struve functions (see table 24).

Table 24

Modified Struve Functions

x	$I_1(x) - L_1(x)$	x	$I_1(x) - L_1(x)$
.0	.0	2.8	.546746
.1	.047930	2.9	.551933
.2	.091990	3.0	.556757
.3	.132480	3.1	.561246
.4	.169710	3.2	.565426
.5	.203952	3.3	.569319
.6	.235457	3.4	.572948
.7	.264454	3.5	.576333
.8	.291151	3.6	.579492
.9	.315740	3.7	.582442
1.0	.338395	3.8	.585199
1.1	.359276	3.9	.587776
1.2	.378530	4.0	.590187
1.3	.396290	4.1	.592445
1.4	.412679	4.2	.594560
1.5	.427810	4.3	.596542
1.6	.441783	4.4	.598402
1.7	.454694	4.5	.600147
1.8	.466629	4.6	.601787
1.9	.477666	4.7	.603328
2.0	.487877	4.8	.604777
2.1	.497329	4.9	.606142
2.2	.506083	5.0	.607426
2.3	.514194	10.0	.630018
2.4	.521712	20.0	.635016
2.5	.528685	50.0	.636385
2.6	.535156	100.0	.636556
2.7	.541164	∞	.636620

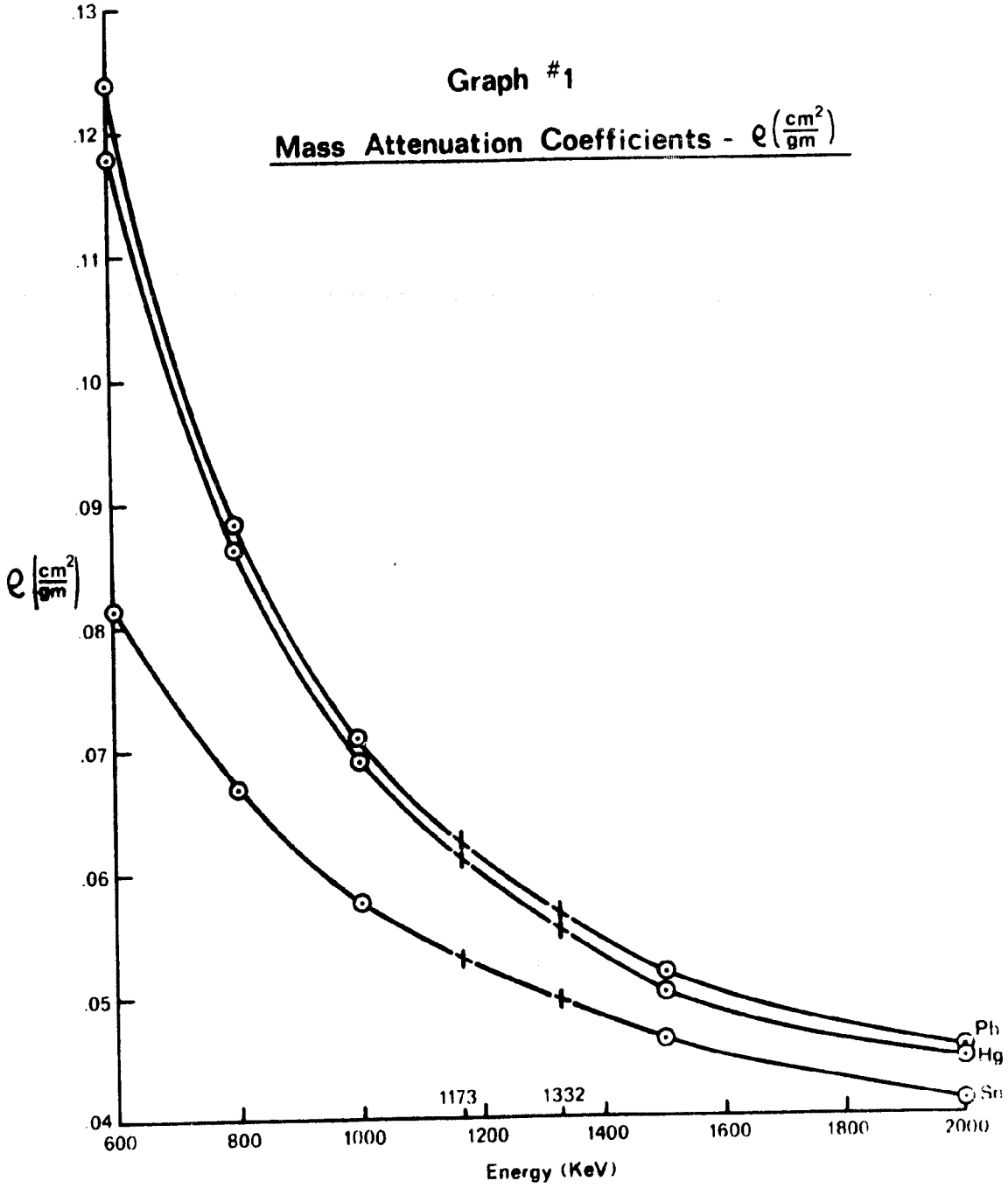
Graph #1
Mass Attenuation Coefficients - ϱ(cm²/gm)
ϱ (cm²/gm)
.13
.12
.11
.10
.09
.08
.07
.06
.05
.04
600
800
1000
1200
1400
1600
1800
2000
1173
1332
Energy (KeV)
Pb
Hg
Sn

Experimental Set Up Showing Scattering Geometry

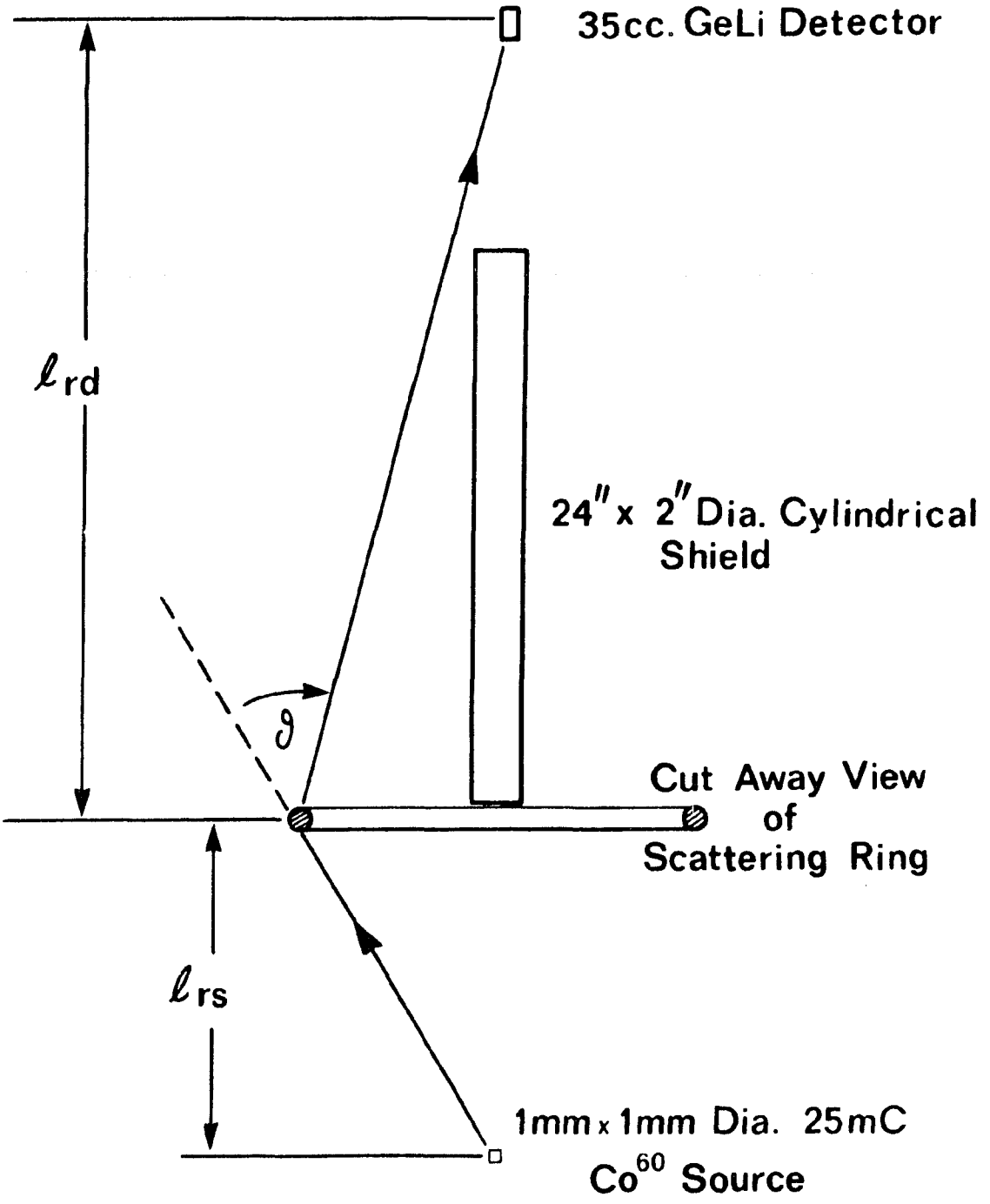

Figure 1

Electronics Block Diagram

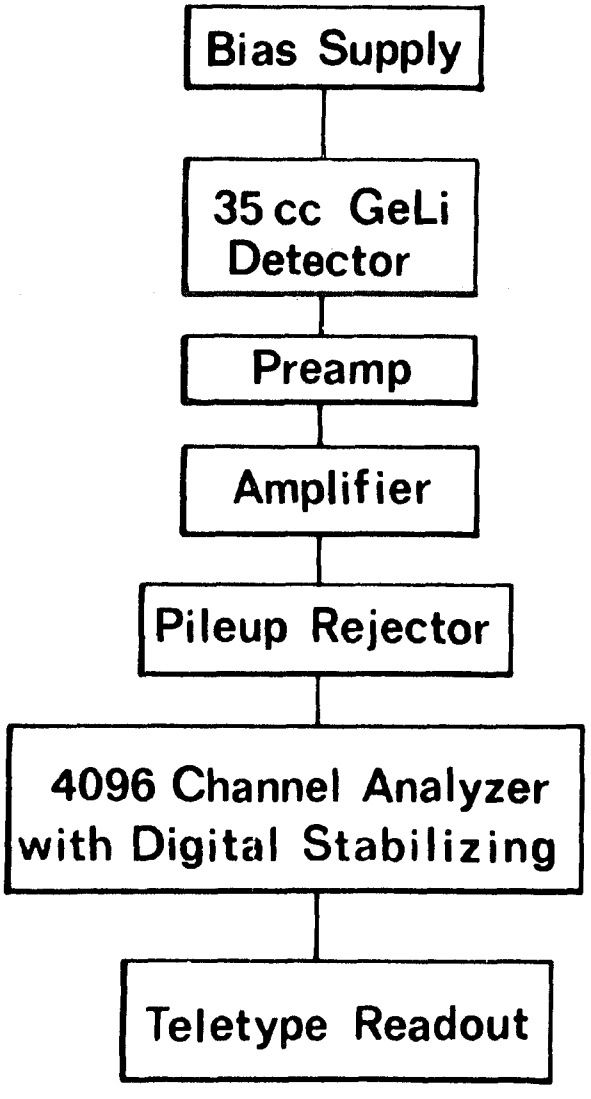

Figure 2

Support System

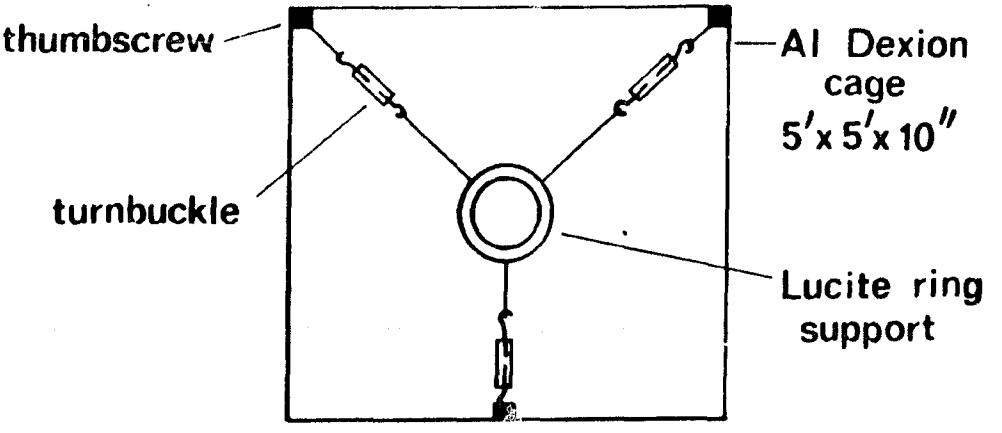

Figure 3

Thumbscrew

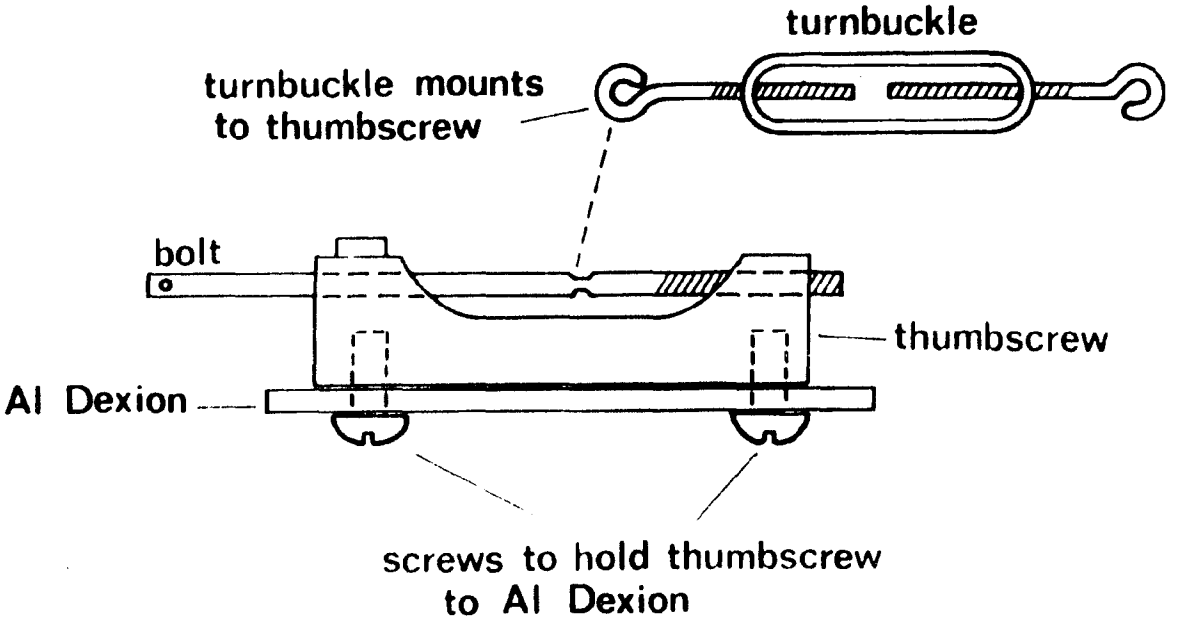

Figure 4

Alignment Disc

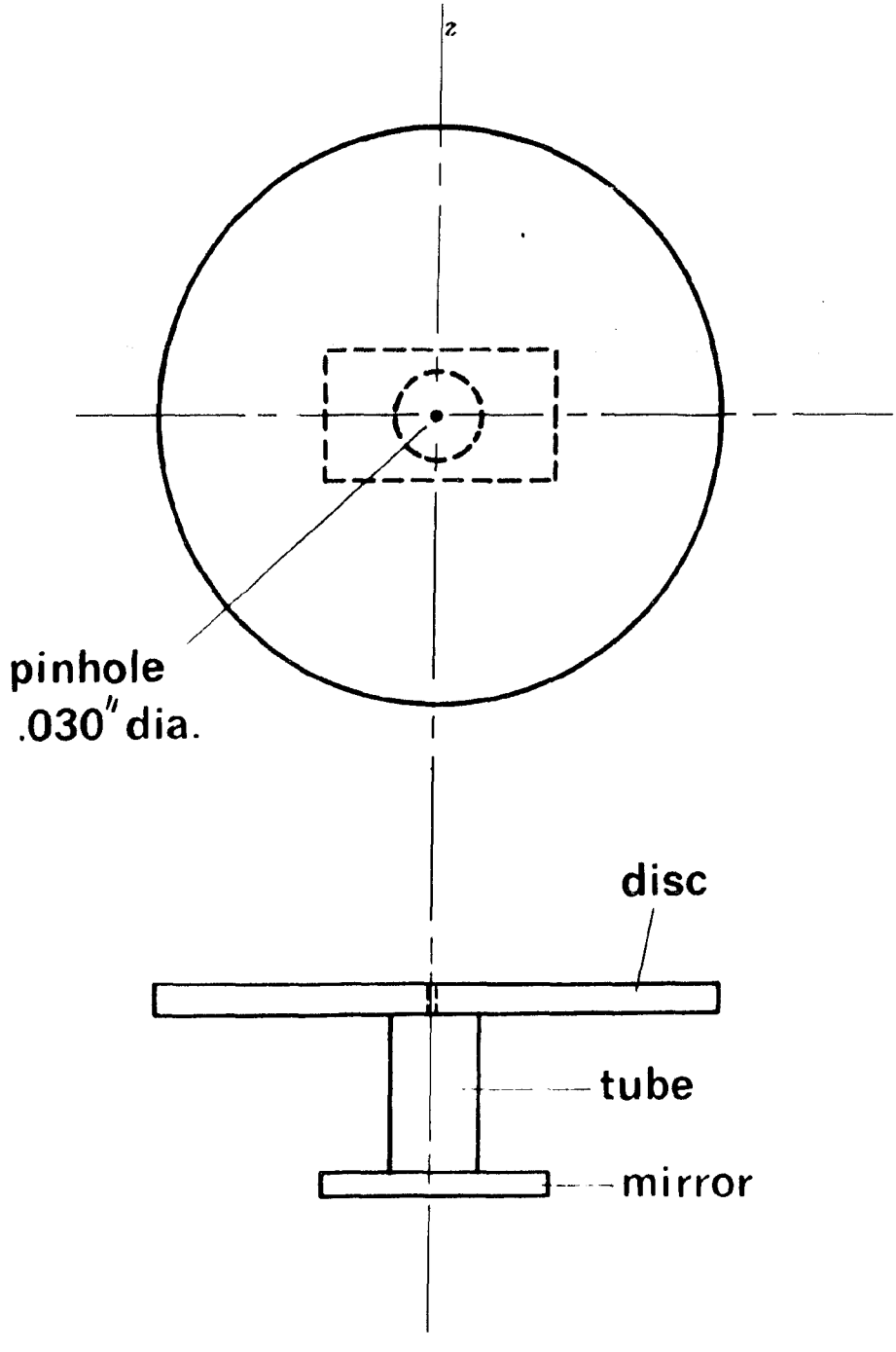

Figure 5

Figure 6. Scan of detector from right front to left front (200 seconds/point)

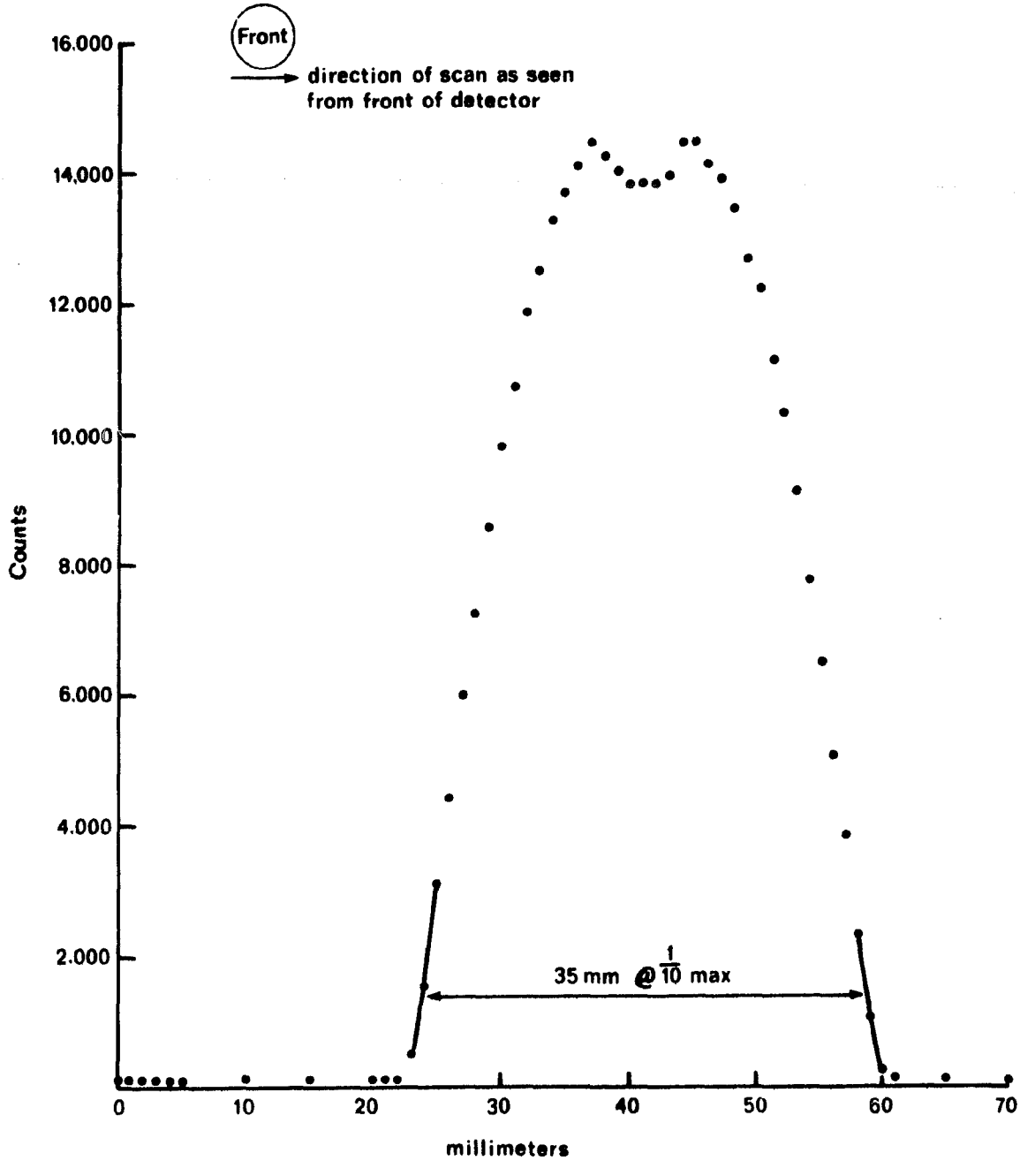

Figure 7. Scan of detector from front bottom to front top (100 sec./point)

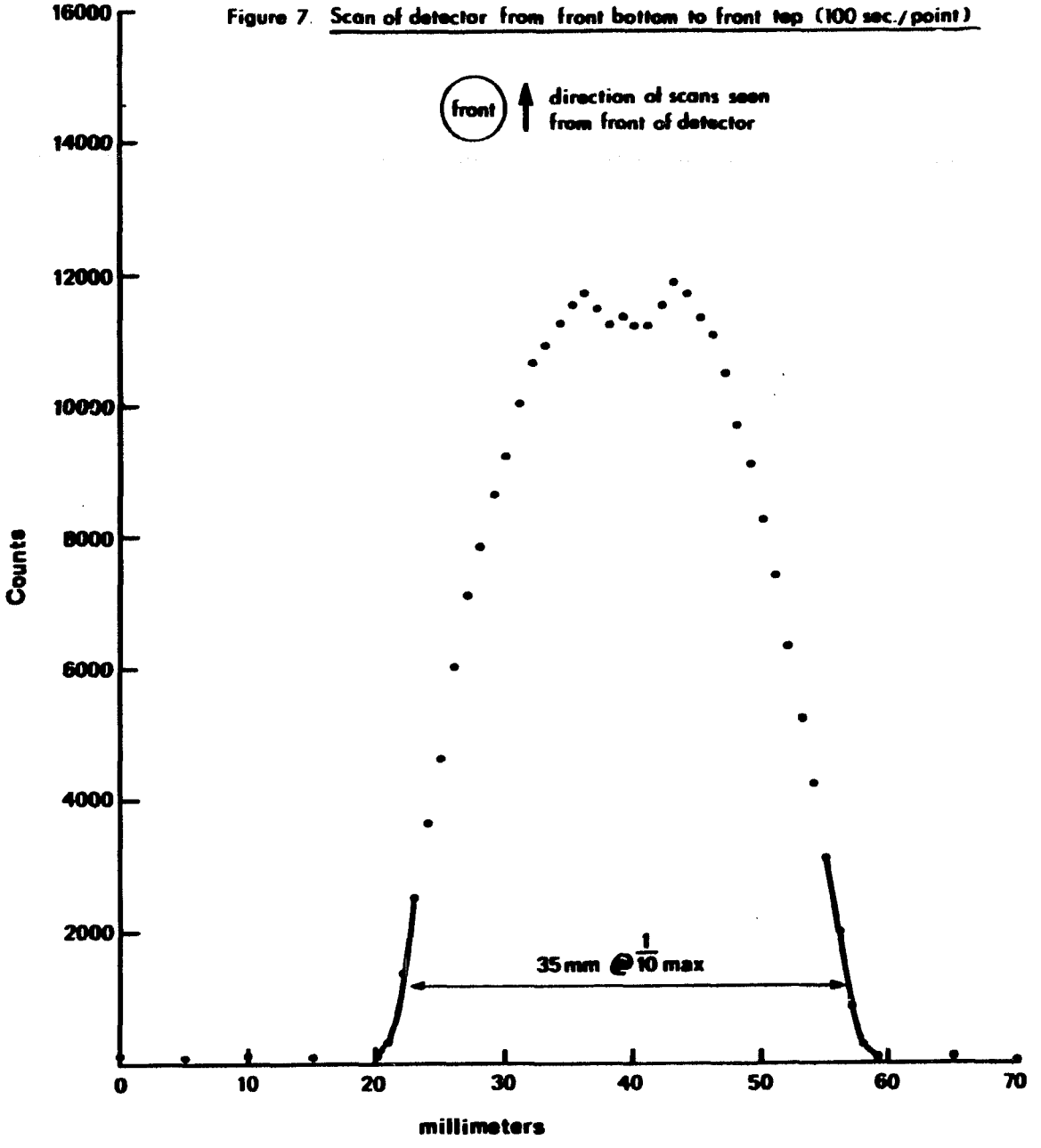

Figure 8 Front to rear scan of detector (200 seconds/point)

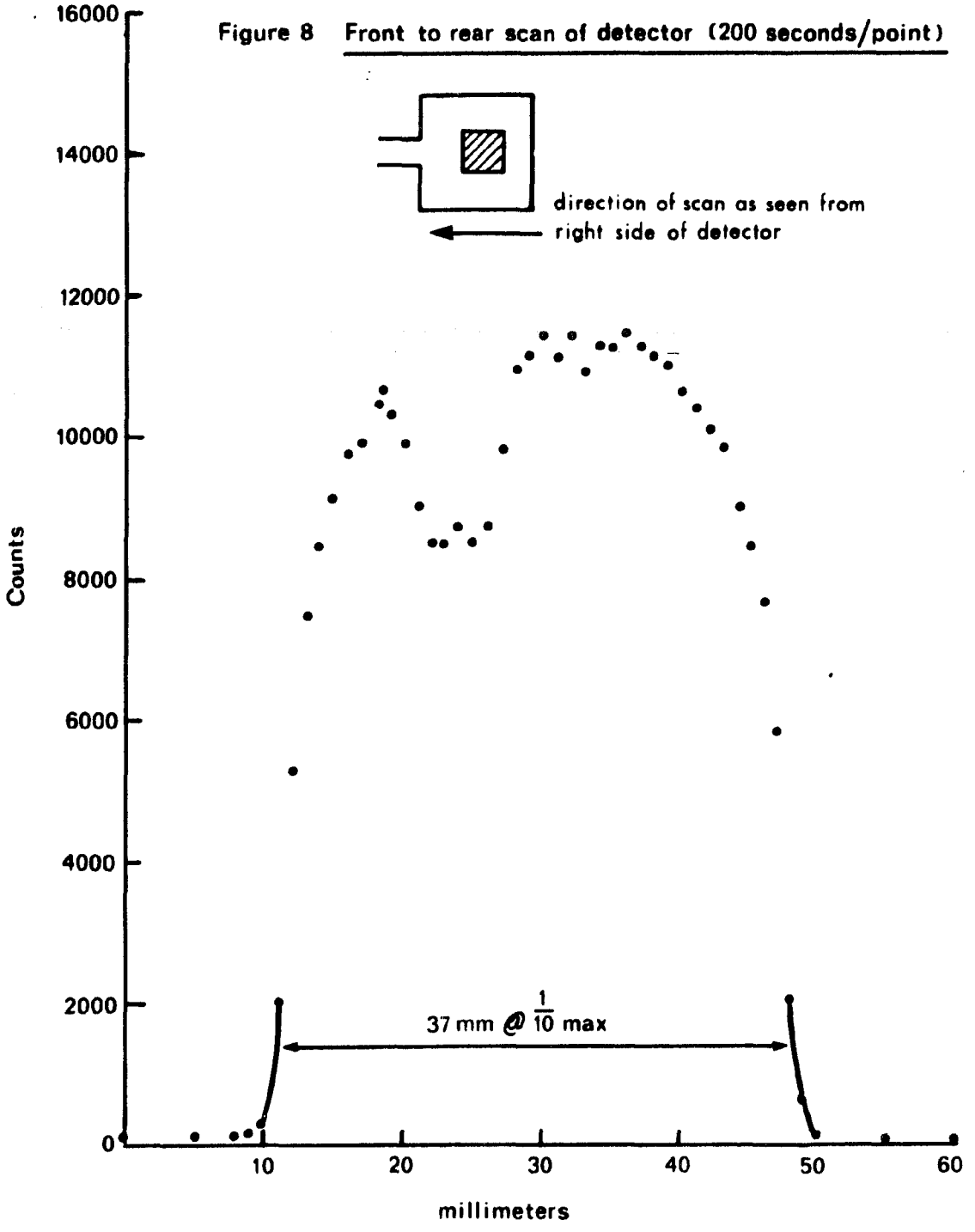

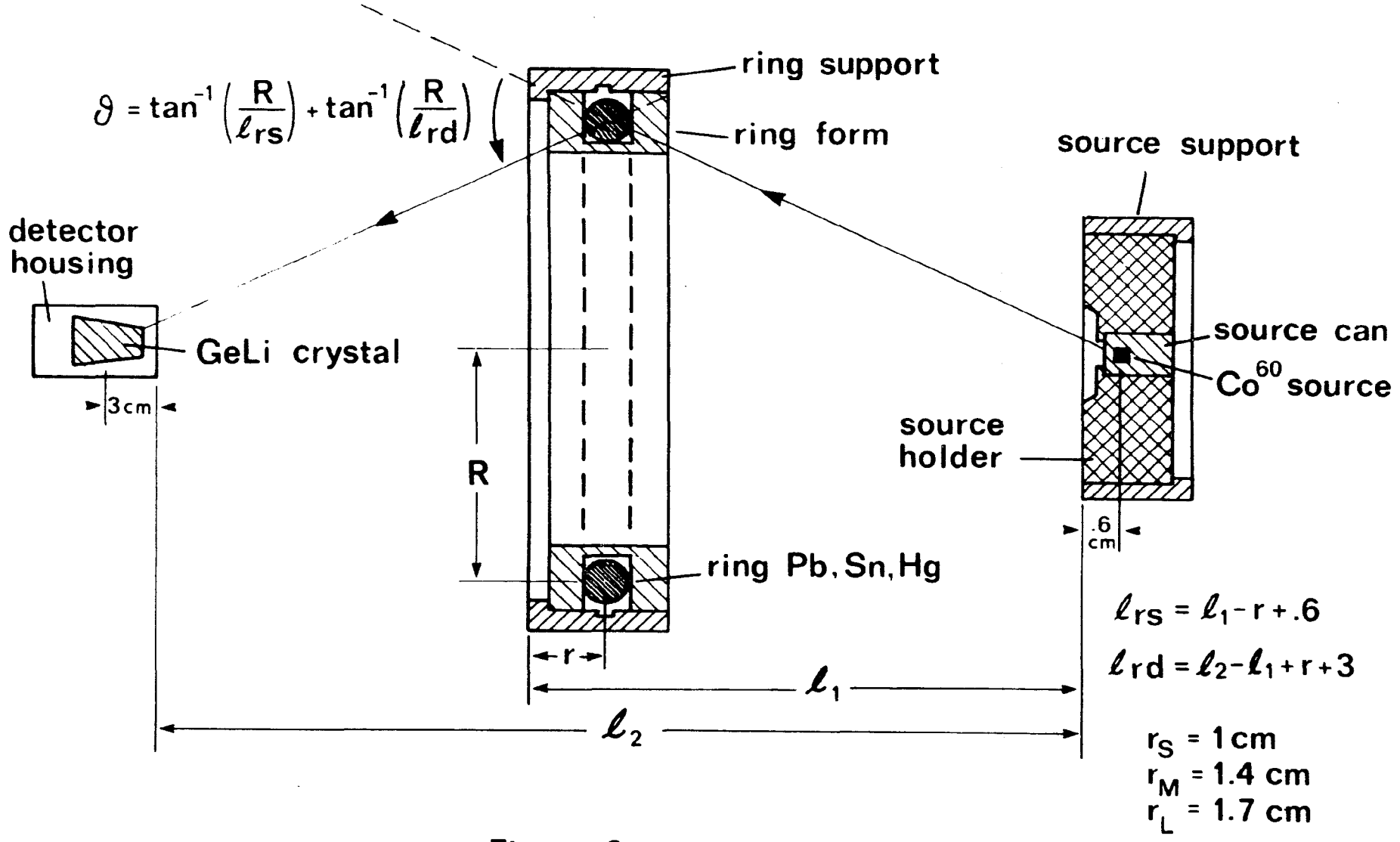
$\vartheta = \tan^{-1}\left(\frac{R}{\ell_{rs}}\right) + \tan^{-1}\left(\frac{R}{\ell_{rd}}\right)$
ring support
ring form
source support
detector housing
GeLi crystal
3cm
source can
Co^{60} source
source holder
R
.6 cm
ring Pb, Sn, Hg
r
ℓ_1
ℓ_2
$\ell_{rs} = \ell_1 - r + .6$
$\ell_{rd} = \ell_2 - \ell_1 + r + 3$
r_S = 1 cm
r_M = 1.4 cm
r_L = 1.7 cm

Figure 9

Data Handling

To find the number of elastic scattering events recorded a ring-in measurement was made followed by a ring-out. The elastic scattering contribution was then the difference of the two runs taken between regions slightly wider than the full energy gamma ray peak.

The ring-out runs were of shorter duration than the ring-in runs and thus had to be time normalized to the rin-in runs. In this respect, the pileup factor had to be checked to see if there was any difference between the two runs. There was no difference.

After time normalization was completed a region near the full energy gamma ray peak but not under the peak, was subtracted from the corresponding region in the ring-in run. The reason was to check if this background truly represented everything in the ring-in run except for the elastic scattering contribution. To within the statistics of the two regions, the difference was zero indicating that the time normalized ring-out run did represent the background contribution to the ring-in run.

Thus, the difference of the two runs was taken to be the elastic scattering contribution. The error in this number was taken to be the sum of the errors in the two regions:

$$N_S = \left[N_{RI} - N_{RO} \right] \left[1 \pm \left(\sqrt{N_{RI}} + \sqrt{N_{RO}} \right) \Big/ \left(N_{RI} - N_{RO} \right) \right]$$

where N_{RI} is the number of counts in the ring-in elastic peak region and N_{RO} is the number of counts in the corresponding ring-out region.

A similar subtraction was made for all other counting measurements.

The errors for the other factors contributing to the differential cross section are all less than three percent and thus the total error is taken to be the error in N_s alone ($\Delta N_s > 10\%$):

$$\frac{d\sigma}{d\Omega} = \frac{d\sigma}{d\Omega}\left[1 \pm \left(\sqrt{N_{RI}} + \sqrt{N_{RO}}\right)/\left(N_{RI} - N_{RO}\right)\right]$$

The error in the scattering angle is less than $\pm$ 2° for the 1/4" diameter ring and $\pm$ 3° for the 1/2" diameter ring. This spread is due to the fact that the source, scatterer and detector are not geometrical points, but rather have finite dimensions.

Results and Conclusions

Graphs 2 to 7 summarize the present work. The dots with the error bars are the experimental points listed in Tables 25 to 30, and the solid curves are the result of the theoretical analysis listed in Tables 31 to 33.

In general, the theoretical analysis yields the same angular dependence for the differential cross section as the experimental results. Each graph can be broken up into three separate regions; (a) for scattering angles less than 15° (ϑ_s), (b) for scattering angles between 15° and 30° (ϑ_m), and (c) for scattering angles greater than 80° (ϑ_l).

For ϑ_s, Rayleigh scattering from the K shell, with no polarization change, dominates the scattering. However, the smaller the scattering angle, the smaller the momentum transfer and thus one expects the higher orbitals, L, M, etc..., to contribute coherently with the K shell contribution. Table 34 shows the angle at which the momentum transfer q ($q = (2E_\gamma/m_ec^2)(\sin\vartheta/2)$, in units of m_ec) equals the characteristic nth shell momentum for each of the two gamma rays of Co^{60}. For smaller scattering angles the momentum transfer is less than the characteristic momentum; as a result, one expects the theoretical calculations in this region to be too small, since only the contribution of the K shell electrons is accounted for. Within the experimental errors (10%), this

is clearly evident, since the curves fall a factor of 1.5 to 2 below the experimental points. Brown and Mayers[1] estimate to K shell contribution to be 80% of the total Rayleigh effect at 1.31 MeV, and that the L shell contributes another 12.5% for all angles. The experimental points at 10° scattering angle are all a factor of 1.25 to 1.75 larger than Brown and Mayers calculation including their L shell estimate of 12.5%. Thus unless there is some systematic error in the experimental points it would appear that the L shell contributes a considerably larger fraction to the scattering than Brown's estimate. In order to clarify this situation a calculation for materials of arbitrary Z, and Co^{60} gamma ray energies, which include the L and M shell in addition to the K shell, should be made.

For θ_m, Rayleigh scattering still dominates, but now the momentum transfers are too large for L or higher orbital contributions to be significant (one expects inelastic rather than elastic scattering from these higher orbitals for $\theta > \theta_s$). Thus the theoretical results should be in agreement with the experimental results. This is the case for lead at 1.33 MeV, although for 1.17 MeV, the experimental points are 30% higher that the theoretical curve. For tin, the theoretical curve is a factor of 10 low, suggesting that the experimentally determined Z dependence of Anand and Sood[2] can not be used to accurately extrapolate the Rayleigh scattering amplitudes from mercury to targets of arbitrary Z. Thus, the excess scattering from lead at 1.17 MeV could be attributable to the

uncertainty of the extrapolation. For mercury the theoretical curves are a factor of 1.5 to 2 low for scattering angles between 40° and 60°. Though there was no extrapolation in Z made, there was one made in energy, from 1.31 MeV to 1.17 MeV. This, however, amounted to a change in the theoretical calculation of less than a percent whereas the experimental points are a factor of 1.5 to 2 larger than the theoretical points. If only the Rayleigh K shell and Nuclear Thomson amplitudes were included, the theoretical points would be 5 to 10 percent lower. It is not clear whether the addition of an L shell contribution of roughly 12.5 percent (of the K shell) would increase or decrease the theoretical points since for larger scattering angles it is expected that the electron contribution from the different shells become incoherent. Therefore, even though there is a variation of 20 percent due to the experimental uncertainty the experimental points are still a factor of 1.25 to 1.5 larger than the theoretical calculations. This difference could be attributable to Delbruck scattering. This same effect has been noted by Dixon et. al.[3], and Hardie et. al.[4,5].

For θ_L, the amplitudes with polarization change dominate over the amplitudes with no polarization change, leading to a near cancellation of the Rayleigh and Nuclear Thomson amplitudes. Thus, even though the L and M shell contributions with polarization change are small (large momentum transfers) compared to the K shell amplitudes, they may be significant enough under these circumstances and should be calculated.

In this region the theoretical curves for lead are in general 20 percent too low and would be 30 percent too low if the Delbruck contribution were neglected (see Tables 35 and 36). However, since the statistical uncertainties are about 30 percent, the theoretical points are well within the experiental error.

It seems clear that there is an increase in scattering above the theoretical prediction (for at least 30° to 60° scattering angle), but whether it is attributable to Delbruck scattering or to the incomplete calculations on Rayleigh scattering will remain an uncertainty until the L shell calculations are carried out for suitable nuclei and gamma ray energies that correspond to those energy sources that are readily available in nature.

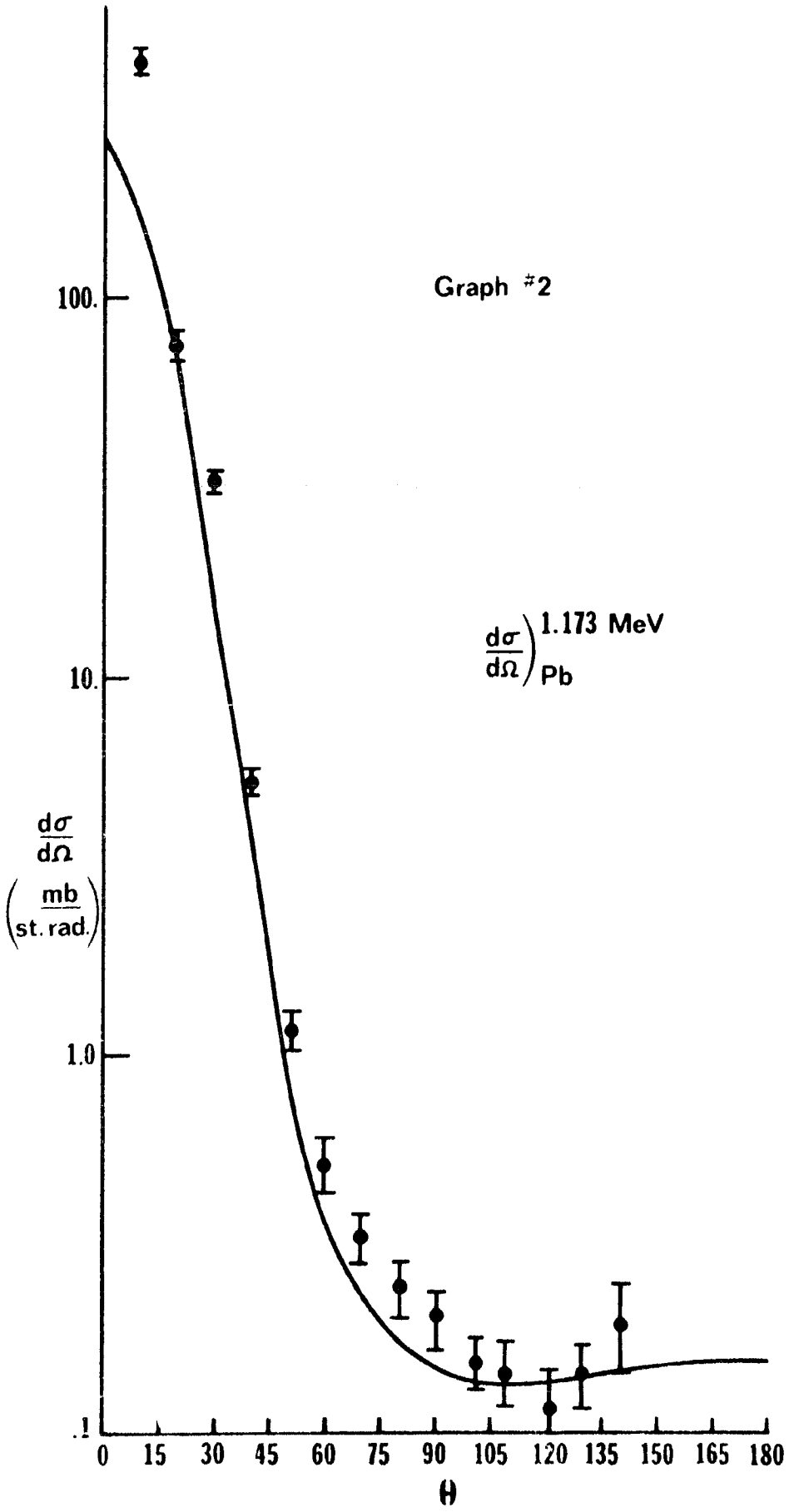
Graph #2
$\left(\frac{d\sigma}{d\Omega}\right)_{Pb}^{1.173\ MeV}$
100.
10.
1.0
.1
$\frac{d\sigma}{d\Omega}\left(\frac{mb}{st.rad.}\right)$
0 15 30 45 60 75 90 105 120 135 150 165 180
θ

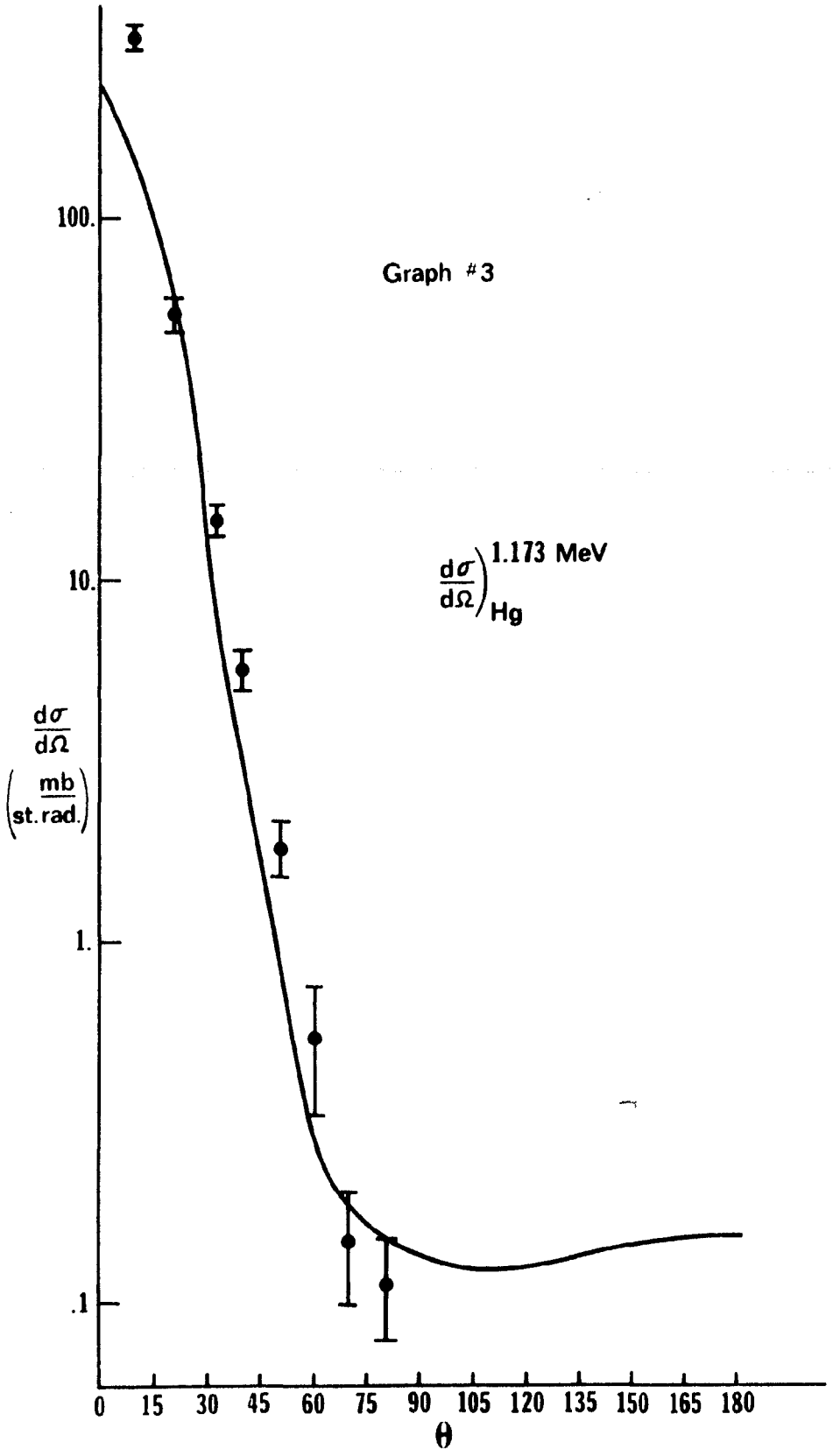
Graph #3
$\left(\frac{d\sigma}{d\Omega}\right)_{Hg}^{1.173\ MeV}$
$\frac{d\sigma}{d\Omega}\left(\frac{mb}{st.rad.}\right)$
100.
10.
1.
.1
0 15 30 45 60 75 90 105 120 135 150 165 180
θ

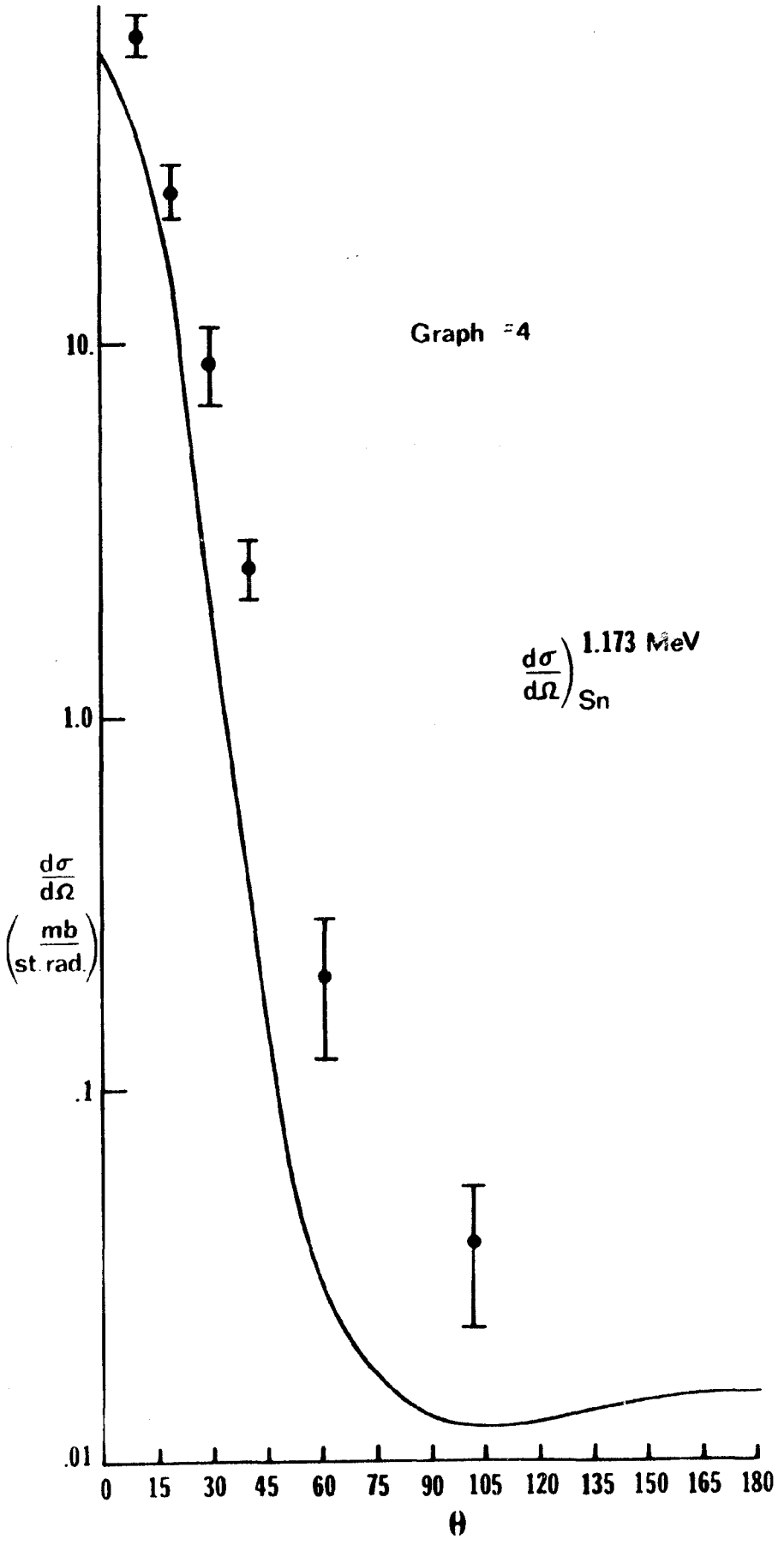
Graph #4
$\left(\frac{d\sigma}{d\Omega}\right)_{Sn}^{1.173\ MeV}$
$\frac{d\sigma}{d\Omega}\left(\frac{mb}{st.\ rad.}\right)$
10.
1.0
.1
.01
0
15
30
45
60
75
90
105
120
135
150
165
180
θ

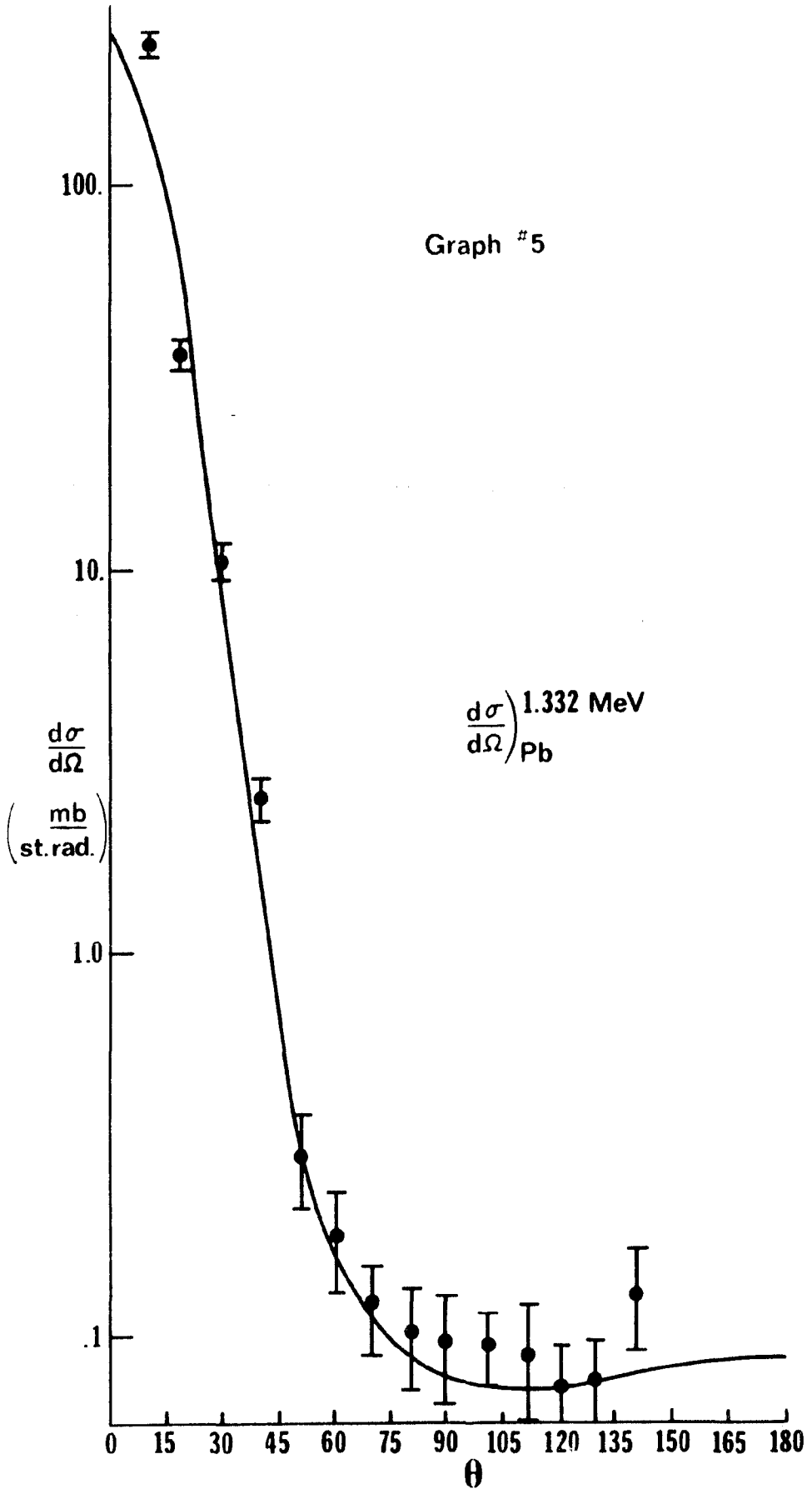
Graph #5
100.
10.
1.0
.1
$\frac{d\sigma}{d\Omega}$
$\left(\frac{mb}{st.rad.}\right)$
$\left(\frac{d\sigma}{d\Omega}\right)_{Pb}$ 1.332 MeV
0
15
30
45
60
75
90
105
120
135
150
165
180
θ

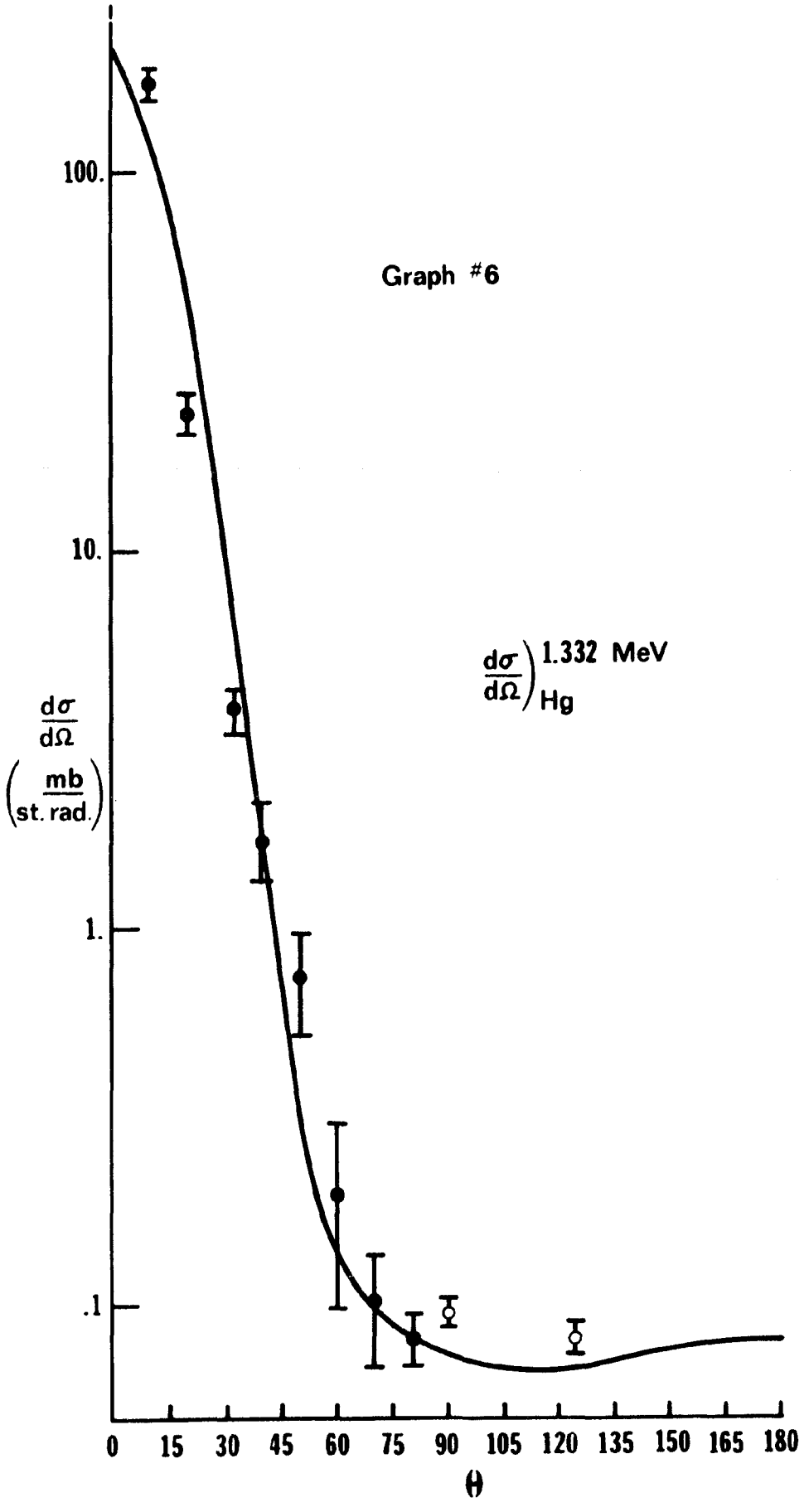
Graph #6
$\frac{d\sigma}{d\Omega}\Big)_{Hg}^{1.332\ MeV}$
$\frac{d\sigma}{d\Omega}\left(\frac{mb}{st.\ rad.}\right)$
100.
10.
1.
.1
0
15
30
45
60
75
90
105
120
135
150
165
180
θ

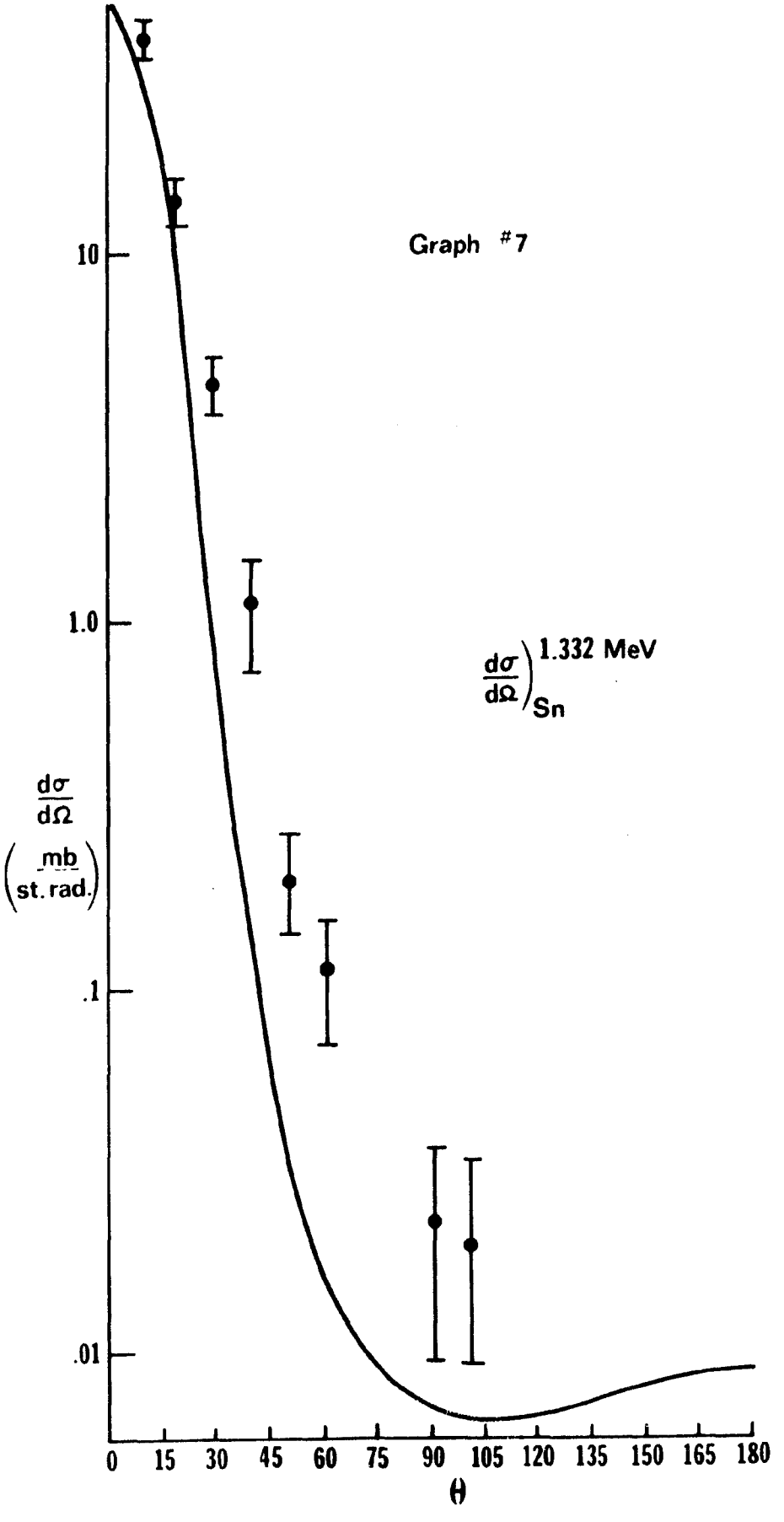
Graph #7
10
1.0
.1
.01
$\frac{d\sigma}{d\Omega}\Big)_{Sn}^{1.332\ MeV}$
$\frac{d\sigma}{d\Omega}$ $\left(\frac{mb}{st.rad.}\right)$
0 15 30 45 60 75 90 105 120 135 150 165 180
θ

Table 25

The Elastic Differential Cross Section for Lead

E_γ = 1.173 MeV

Θ	N_S	$N_{O\epsilon}(10^8)$	$R^2+1_{rs}^2$	P	$N_{OS}(10^{13})$	N_ϵ	$N(10^{23})$	A	$\frac{d\sigma}{d\Omega}$ (mb/St. Rad.)
10±1	30456	12.53	4537	1.47	9.42	25954	3.46	.711	423. ±25.
19±1	7740	15.29	378	1.47	4.09	8667	3.46	.712	75.3 ±6.
29±1	3579	3.33	981	1.48	2.72	3879	6.95	.712	33.1 ±1.7
40±1	1982	2.54	389	1.51	5.16	2160	6.95	.713	5.33 ± .43
51±2	1700	11.62	256	1.58	10.81	12779	6.95	.714	1.17 ± .12
61±2	1039	12.82	1254	1.66	8.10	20381	62,67	.522	.517± .083
70±3	1265	12.82	906	1.69	11.03	20381	62.67	.525	.336± .047
80±3	1469	12.82	696	1.65	13.28	20381	62.67	.527	.242± .012
91±3	1341	12.82	584	1.68	12.21	20381	62.67	.530	.204± .037
101±3	1196	12.82	529	1.66	12.90	20381	62.67	.529	.154± .022
109±3	1129	12.82	512	1.71	12.96	20381	62,67	.528	.145± .025
121±3	729	1.82	534	1.66	13.25	2293	62.67	.527	.117± .029
130±3	1135	1.82	581	1.64	17.95	2293	62.67	.526	.145± .026
140±3	597	2.44	717	1.55	11.69	2136	62.67	.526	.197± .053

Table 26

The Elastic Differential Cross Section for Lead

E_γ = 1.33 MeV

θ	N_S	$N_{0\epsilon}(10^3)$	$R^2+1_{TS}^2$	P	$N_{0S}(10^3)$	N_ϵ	$N(10^{23})$	A	$\frac{d\sigma}{d\Omega}$ (mb/St. Rad)
10±1	15036	12.53	4537	1.47	9.42	22131	3.46	.733	237.6 ±13.8
19±1	3383	15.29	378	1.47	4.09	7546	3.46	.734	36.67 ± 2.93
29±1	989	3.33	981	1.48	2.72	3266	6.95	.735	10.5 ± .8
40±1	809	2.54	389	1.51	5.16	1801	6.95	.736	2.54 ± .30
51±2	416	11.62	256	1.58	10.81	11857	6.95	.736	.298± .084
61±2	347	12.82	1254	1.66	8.10	17978	62.67	.554	.183± .053
70±3	425	12.82	906	1.69	11.03	17978	62.67	.556	.121± .034
80±3	588	12.82	696	1.65	13.28	17978	62.67	.558	.104± .030
91±3	597	12.82	584	1.68	12.21	17978	62.67	.561	.097± .031
101±3	691	12.82	529	1.66	12.90	17978	62.67	.560	.096± .021
112±3	425	1.31	518	1.71	17.24	910	62.67	.559	.090± .031
121±3	473	1.82	534	1.66	13.25	2212	62.67	.557	.075± .019
130±3	615	1.82	581	1.64	17.95	2212	62.67	.556	.077± .022
140±3	397	2.44	717	1.55	11.69	2029	62.67	.555	.130± .038

Table 27

The Elastic Differential Cross Section for Mercury

E_γ = 1.173 MeV

θ	N_S	$N_{0\epsilon}(10^8)$	$R^2+1^2_{rs}$	P	$N_{0S}(10^{13})$	N_ϵ	$N(10^{23})$	A	$\frac{d\sigma}{d\Omega}$ (mb/St. Rad.)
10 ± 1	10470	2.01	4424	1.23	14.98	2929	1.001	.816	319.5 ± 24.6
20 ± 2	4778	1.52	329	1.22	10.90	602	1.001	.817	54.2 ± 5.2
32 ± 1	5510	2.00	1352	1.46	15.24	5609	2.125	.817	14.7 ± 1.2
40 ± 2	2628	1.20	483	1.38	15.60	1363	2.125	.818	$5.69 \pm .66$
50 ± 2	1371	1.40	275	1.34	16.49	1347	2.125	.819	$1.83 \pm .29$
60 ± 2	684	1.11	201	1.30	23.05	927	2.125	.820	$.541 \pm .212$
70 ± 3	827	1.41	860	1.40	22.38	1949	37.08	.561	$.151 \pm .047$
80 ± 3	1070	1.40	677	1.39	28.18	2101	37.08	.564	$.114 \pm .034$

Table 28

E_γ = 1.332 MeV

θ	N_S	$N_{0\epsilon}(10^8)$	$R^2+1^2_{rs}$	P	$N_{0S}(10^{13})$	N_ϵ	$N(10^{23})$	A	$\frac{d\sigma}{d\Omega}$ (mb/St. Rad.)
10 ± 1	5223	2.01	4424	1.23	14.98	2667	1.001	.831	171.9 ± 12.4
20 ± 2	1630	1.52	329	1.22	10.90	464	1.001	.832	23.6 ± 2.4
32 ± 1	738	2.00	1352	1.46	9.57	4397	2.125	.833	$3.91 \pm .36$
40 ± 2	771	1.20	483	1.38	15.60	1268	2.125	.834	$1.76 \pm .39$
50 ± 2	495	1.40	275	1.34	16.49	1173	2.125	.835	$.744 \pm .223$
60 ± 2	225	1.11	201	1.30	23.05	805	2.125	.835	$.198 \pm .101$
70 ± 3	502	1.41	860	1.40	22.38	1691	37.08	.591	$.103 \pm .033$
80 ± 3	799	1.40	677	1.39	28.18	2101	37.08	.593	$.081 \pm .012$

Table 29

The Elastic Differential Cross Section for Tin

E_γ = 1.173 MeV

θ	N_S	$N_{0\epsilon}(10^8)$	$R^2+I_{TS}^2$	P	$N_{0S}(10^{13})$	N_ϵ	$N(10^{23})$	A	$\frac{d\sigma}{d\Omega}$ (mb/St.Rad)
10±1	6349	12.53	4537	1.47	9.42	25954	3.88	.827	67.7 ±6.4
19±1	5301	15.29	378	1.47	6.26	8667	3.88	.828	26.4 ±4.0
29±1	1308	3.33	981	1.48	2.72	3879	7.90	.829	9.10 ±1.00
40±1	1258	2.54	389	1.51	5.16	2160	7.90	.830	2.57 ± .49
61±1	620	12.82	1254	1.66	8.10	20381	70.81	.696	.202± .077
101±3	448	12.82	529	1.66	12.9	20381	70.81	.700	.039± .017

Table 30

E_γ = 1.332 MeV

θ	N_S	$N_{0\epsilon}(10^8)$	$R^2+I_{TS}^2$	P	$N_{0S}(10^{13})$	N_ϵ	$N(10^{23})$	A	$\frac{d\sigma}{d\Omega}$ (mb/St.Rad.)
10±1	3179	12.53	4537	1.47	4.40	22131	3.88	.837	39.3 ±4.3
19±1	2521	15.29	378	1.47	6.26	7546	3.88	.837	14.0 ±2.0
29±1	532	3.33	981	1.48	2.72	3206	7.90	.838	4.46 ± .09
40±1	469	2.54	389	1.51	5.16	1801	7.90	.838	1.14 ± .35
51±1	359	11.61	256	1.58	10.81	11857	7.90	.838	.199± .060
61±1	309	12.82	1254	1.66	8.10	17978	70.81	.715	.111± .041
91±3	202	12.82	584	1.68	12.90	17978	70.81	.721	.023± .016
101±3	205	12.82	529	1.66	12.96	17978	70.81	.718	.020± .014

Table 31

Results of Theoretical Calculations for Lead

ϑ	E_γ = 1.173 MeV Total Amplitude $a^{NF}(R_o)$	$a^{F}(R_o)$	$\frac{d\sigma}{d\Omega}$ (mb/St.Rad.)	E_γ = 1.332 MeV Total Amplitude $a^{NF}(R_o)$	$a^{F}(R_o)$	$\frac{d\sigma}{d\Omega}$ (mb/St.Rad.)
0	-1.796 +.2544i	0	261.2	-1.7542+.0719i	0	244.7
15	-1.1610+.0176i	.0282-.0022i	107.1	-1.065 +.0509i	.0285-.006 i	90.33
30	- .4181+.0088i	.0536-.0042i	14.12	- .324 +.0219i	.0451-.0118i	8.546
45	- .1337+.0056i	.0531-.0036i	1.647	- .0881+.0141i	.0412-.0101i	.7749
60	- .0397+.0044i	.0485-.0027i	.3140	- .0248+.0112i	.0271-.0074i	.1215
75	- .0093+.0037i	.0493-.0019i	.2012	- .0117+.0095i	.0363-.0057i	.1252
90	- .0036+.0026i	.0428-.0013i	.1471	- .0008+.0069i	.0312-.0039i	.0823
105	- .0001+.002 i	.0428-.0011i	.1459	+.0053i	.031 -.0036i	.0796
120	- .0034+.0013i	.0432-.0009i	.1493	.0006+.0036i	.0317-.003 i	.0816
135	- .0016+.0005i	.0426-.0014i	.1445	.ooo3+.0015i	.0309-.0036i	.0770
150	- .0007+.0004i	.0437-.0013i	.1518	.0002+.0011i	.0321-.0033i	.0828
165	.0002+.0002i	.044 -.0012i	.1538	.0008+.0006i	.0324-.0031i	.0842
180	0	.0443-.0013i	.1560	0	.0332-.0035i	.0885

Table 32

Results of Theoretical Calculations for Mercury

	E_γ = 1.173 MeV			E_γ = 1.332 MeV		
	Total Amplitude			Total Amplitude		
θ	$a^{NF}(R_o)$	$a^{F}(R_o)$	$\frac{d\sigma}{d\Omega}\left(\frac{mb}{St.Rad.}\right)$	$a^{NF}(R_o)$	$a^{F}(R_o)$	$\frac{d\sigma}{d\Omega}\left(\frac{mb}{St.Rad.}\right)$
0	-1.6960+.0240i	0	228.4	-1.6560+.0678i	0	218.1
15	-1.0955+.0166i	.0266-.0021i	95.37	-1.0057+.0480i	.0256-.0057i	80.54
30	- .3950+.0083i	.0506-.0034i	12.60	- .3063+.0207i	.0427-.0111i	10.65
45	- .1265+.0053i	.0499-.0034i	1.471	- .0836+.0133i	.0389-.0075i	.6963
60	- .0329+.0042i	.0460-.0025i	.2558	- .0239+.0106i	.0298-.0070i	.1287
75	- .0091+.0035i	.0467-.0018i	.1810	- .0063+.0089i	.0338-.0054i	.1025
90	- .0037+.0025i	.0407-.0012i	.1332	- .0011+.0065i	.0281-.0037i	.0718
105	- .0001+.0021i	.0407-.0010i	.1320	.0002+.0052i	.0296-.0034i	.0726
120	- .0033+.0016i	.0412-.0008i	.1359	.0004+.0034i	.0304-.0028i	.0749
135	- .0015+.0005i	.0407-.0013i	.1319	.0002+.0014i	.0296-.0034i	.0706
150	- .0007+.0004i	.0419-.0012i	.1396	.0001+.0010i	.0309-.0031i	.0767
165	- .0002+.0002i	.0421-.0011i	.1408	.0007+.0006i	.0312-.0029i	.0780
180	0	.0425-.0012i	.1435	0	.0320-.0033i	.0822

Table 33

Results of Theoretical Calculations for Tin

	E_γ = 1.173 MeV			E_γ = 1.332 MeV		
	Total Amplitude			Total Amplitude		
θ	$a^{NF}(R_0)$	$a^{F}(R_0)$	$\frac{d\sigma}{d\Omega}\left(\frac{mb}{St.Rad.}\right)$	$a^{NF}(R_0)$	$a^{F}(R_0)$	$\frac{d\sigma}{d\Omega}\left(\frac{mb}{St.Rad.}\right)$
0	-.8798+.0125i	0	61.45	-.8098+.0322i	0	52.17
15	-.5676+.0086i	.0138-.0011i	25.60	-.4911+.0235i	.0125-.0028i	19.21
30	-.1425+.003 i	.0183-.0015i	1.640	-.1015+.0069i	.0143-.0037i	.8391
45	-.0401+.0017i	.0158-.0010i	.1478	-.0252+.0040i	.0117-.0028i	.0632
60	-.0121+.0013i	.0139-.0007i	.0155	-.0078+.0030i	.0100-.0019i	.0138
75	-.0035+.0011i	.0139-.0005i	.0164	-.0027+.0026i	.0102-.0015i	.0096
90	-.0018+.0007i	.0124-.0003i	.0125	-.0011+.0018i	.0092-.0009i	.0071
105	-.0006+.0006i	.0130-.0002i	.0135	-.0006+.0015i	.0097-.0009i	.0077
120	-.0014+.0003i	.0133-.0002i	.0142	-.0003+.0010i	.0102-.0008i	.0084
135	-.0007+.0001i	.0132-.0004i	.0139	-.0002+.0004i	.0099-.0010i	.0079
150	-.0003+.0001i	.0136-.0003i	.0147	-.0001+.0003i	.0104-.0009i	.0087
165	.0000+.0001i	.0137-.0003i	.0149	-.0002+.0002i	.0105-.0008i	.0088
180	0	.0139-.0003i	.0153	0	.0108-.0010i	.0093

Table 34

The Scattering Angle (θ), For Which The Momentum Transfer (q), Is Equal To The Characteristic Electron Momentum (P_n)

		K shell	L shell	M shell	N shell	O shell
Pb	$q=P_n$ (m_ec)	.6	.3	.2	.15	.12
	θ(1.17 MeV)	15°	7.5°	5°	3.75°	3°
	θ(1.33 MeV)	13.5°	6.5°	4.5°	3.25°	2.5°
Hg	$q=P_n$ (m_ec)	.584	.292	.195	.146	.117
	θ(1.17 MeV)	14.5°	7.25°	5°	3.75°	3°
	θ(1.33 MeV)	13°	6.5°	4.25°	3.25°	2.5°
Sn	$q=P_n$ (m_ec)	.365	.183	.122	.091	.073
	θ(1.17 MeV)	9°	4.5°	3°	2.25°	1.75°
	θ(1.33 MeV)	8°	4°	2.75°	2°	1.5°

(where $\theta=2\sin^{-1}[(q/2)(m_ec^2/E_\gamma)]$)

Table 35

$\frac{d\sigma}{d\Omega}\left(\frac{mb}{St.Rad.}\right)$ for E_γ = 1.173 MeV

θ	Mercury		Lead		Tin	
	R+T+D	R+T	R+T+D	R+T	R+T+D	R+T
75	.1810	.1728	.2012	.1917	.0164	.0148
90	.1332	.1259	.1417	.1387	.0125	.0116
105	.1320	.1243	.1459	.1372	.0135	.0125
120	.1359	.1283	.1493	.1407	.0142	.0132

Table 36

$\frac{d\sigma}{d\Omega}\left(\frac{mb}{St.Rad.}\right)$ for E_γ = 1.332 MeV

θ	Mercury		Lead		Tin	
	R+T+D	R+T	R+T+D	R+T	R+T+D	R+T
75	.1025	.0947	.1252	.1134	.0096	.0088
90	.0718	.0648	.0823	.0711	.0071	.0064
105	.0726	.0654	.0796	.0717	.0077	.0069
120	.0749	.0676	.0816	.0735	.0084	.0075

Appendix

Number

1 Brown and Mayers, Proc. Roy. Soc. (Lon.), A242, 89 (1957)

2 Anand and Sood, Nucl. Phys., 73, 368 (1963)

3 Dixon and Storey, Can. Jour. Phys., 46, 1153 (1963)

4 Hardie, Merrow, and Schwandt, Phys. Rev., 1, 714 (2/70)

5 Hardie, DeVries, and Chiang, Phys. Rev., 3, 1287 (3/71)